Geochimica et Cosmochimica Acta, Vol. 69, No. 7, pp. 1721–1737, 2005

0016-7037/05 $30.00 + .00

doi:10.1016/j.gca.2004.06.027

Solid solutions of trace Eu(III) in calcite: Thermodynamic evaluation of experimental data over a wide range of pH and pCO_2

E. Curti,* D. A. Kulik and J. Tits

Laboratory for Waste Management, Paul Scherrer Institute, 5323 Villigen PSI, Switzerland

(*Received January* 23, 2004; *accepted in revised form June* 23, 2004)

Abstract—The thermodynamics of dilute Eu-calcite solid solutions formed under widely different pH-pCO_2 conditions at $T = 25°C$ and $p = 1$ bar were investigated using three sets of Eu(III) uptake experiments, two of which were taken from the literature: (a) recrystallization in synthetic cement pore water at pH $\sim$ 13 and $pCO_2 \sim 10^{-13}$ bar (this work); (b) coprecipitation in 0.1 M $NaClO_4$ at pH $\sim$ 6 and $pCO_2 \sim 1$ bar; (c) coprecipitation in synthetic seawater at pH $\sim$ 8 and pCO_2 ranging from 3×10^{-4} to 0.3 bar.

Solid solution formation was modeled using the Gibbs energy minimization (GEM) method. In a first step ("forward" modeling), we tested ideal binary solid solution models between calcite and the Eu end-members $Eu_2(CO_3)_3$, $EuNa(CO_3)_2$, $Eu(OH)CO_3$ or $Eu(OH)_3$, for which solids with independently measured solubility products exist. None of these four binary solid solutions was capable of reproducing all three experimental datasets simultaneously. In a second step ("inverse" modeling), ideal binary solid solutions were constructed between calcite and the candidate Eu end-members $EuO(OH)$, $EuH(CO_3)_2$ and $EuO(CO_3)_{0.5}$, for which no independent solubility products are available. For each single data point and each of these end-members, a free energy of formation with inherent activity coefficient term ($G^*_\alpha = G^o_\alpha + RT \ln\gamma_\alpha$) was estimated from "dual thermodynamic" GEM calculations. The statistical mean of G^*_α was then calculated for each of the three datasets. A specific end-member was considered to be acceptable if a standard deviation of $\pm$ 2 kJ mol^{-1} or less resulted for each single dataset, and if the mean G^*_α-values calculated for the three datasets coincided. No binary solid solution with any of the seven above mentioned end-members proved to satisfy these criteria.

The third step in our analysis involved consideration of ternary solid solutions with $CaCO_3$ as the major end-member and any two of the seven considered Eu trace end-members. It was found that the three datasets can only be reproduced simultaneously with the ternary ideal solid solution $EuH(CO_3)_2$ – $EuO(OH)$ – $CaCO_3$, setting $G^*_{EuH(CO3)2} = -1773$ kJ mol^{-1} and $G^*_{EuO(OH)} = -955$ kJ mol^{-1}, whereas all other end-member combinations failed. Our results are consistent with time-resolved laser fluorescence data for Cm(III) and Eu(III) indicating that two distinct species are incorporated in calcite: one partially hydrated, the other completely dehydrated. In conclusion, our study shows that substitution of trivalent for divalent cations in carbonate crystal structures is a more complex process than the classical isomorphic divalent-divalent substitution and may need consideration of multicomponent solid solution models. *Copyright © 2005 Elsevier Ltd*

1. INTRODUCTION

1.1. Background

The mobilization of toxic pollutants from nuclear and conventional waste repositories may threaten the safety of humans and other life forms. Fortunately, chemical retention processes will often reduce the flux of contaminants to the biosphere. Accordingly, engineered barriers with favorable properties are commonly foreseen in the design of waste disposal facilities. For instance, some nuclear waste repository concepts rely on the adsorption capacity of bentonite backfills (NAGRA, 2002; SKB, 1999).

Although the formation of solid solutions has long been recognized as a mechanism of contaminant retention, this process, in contrast to adsorption, is seldom considered in safety assessments for repository sites. Two reasons for this oversight are (i) the inherent complexity of thermodynamic solid solution models and (ii) the lack of experimental parameters necessary for a quantitative treatment.

In some cases, contaminant sequestration can be successfully modeled as a binary mixture of two isomorphous end-members with known solubility products, but the structure and stoichiometry of the minor end-member (representing the contaminant) are often unknown. Specifically, most radionuclides do not form solids that are fully isomorphic with common host minerals like clays, carbonates, sulfates, hydroxides, and calcium silicate hydrates in cement systems. The major cations in these host minerals are monovalent or divalent (alkali, alkaline earths and transition metals) whereas actinides, e.g., Am(III), Cm(III), Pu(III/IV/VI), U(III,IV,VI), Np(IV/V/VI), Th(IV) and fission products like Tc(IV), Se(IV/VI), Sn(IV), Zr(IV) have higher valencies. Consequently, the coordinative environment of most radionuclides in common secondary phases will probably differ from that of the substituted major cation.

1.2. Homovalent and Heterovalent Substitution

In addition to possible deformations induced by differences in ionic radii, the problem of local charge balance has to be considered. For example, substitution of Am^{3+} or Th^{4+} for Ca^{2+} in calcite leads to an excess of positive charge in the vicinity of the

* Author to whom correspondence should be addressed (enzo.curti@psi.ch).

substituted ion, which must be compensated. There are three fundamental mechanisms providing local charge balance: (i) coupled ion substitution; (ii) ion substitution adjacent to a vacant site; and (iii) coordinative rearrangements. The first mechanism can be exemplified by the substitution of two adjacent Ca^{2+} ions by one Eu^{3+} and one Na^{+} ion in the lattice. The second mechanism can be illustrated by the substitution of two Eu^{3+} ions and one vacant cation site for three contiguous Ca^{2+} ions. Finally, the third mechanism calls for a lattice deformation and changes in the local coordination environment of the substituted ion, so that charge is balanced on a local scale. For instance, as an alternative to mechanism (ii), an entire $Ca_3(CO_3)_3$ group could be replaced by a single electroneutral $Eu_2(CO_3)_3$ group with a structure differing from that of pure calcite, inducing a localized lattice strain. As a result, the third (vacant) octahedral site would be eliminated and the number of coordinating CO_3^{2-} groups per cation would increase.

From the preceding considerations, it follows that there is no obvious solution to the problem of predicting the correct stoichiometry and structure for a minor end-member in the case of heterovalent substitution. In turn, this complicates the thermodynamic modeling of such solid solutions (see e.g., McIntire, 1963).

1.3. Outline and Objectives of this Study

In the past years, special attention has been paid to the study of chemical reactions between rare-earth elements (REE) and minerals/rocks in conjunction with nuclear waste disposal. Besides being part of the radioactive waste inventory, light REEs like Eu(III) and Nd(III) are frequently used as analogues of long-lived trivalent actinides (^{243}Am, ^{245}Cm, and ^{246}Cm), which contribute considerable α-activities in high-level radioactive waste (NAGRA, 2002; SKB, 1999).

In this study, we investigate the interaction of trace amounts of Eu(III) with calcite, using three sets of experiments carried out under widely different conditions and with different techniques. The first set includes experiments performed in our laboratory with artificial cement pore water (ACW) presaturated with calcite and portlandite at pH $\sim$ 13. In this medium, predefined amounts of tracer-free calcite were allowed to recrystallize in the presence of different initial concentrations of ^{152}Eu tracer for two weeks. In the second set of experiments, carried out by Lakshtanov and Stipp (2004) using the pH-stat technique described by Tesoriero and Pankow (1996), calcite was precipitated from oversaturated solutions at pH $\sim$ 6 and $pCO_2 = 1$ bar in the presence of varying amounts of dissolved Eu. The third set considered in this study is a series of coprecipitation experiments performed in synthetic seawater at pH $\sim$ 8 and pCO_2 ranging from 3×10^{-4} to 0.3 bar (Zhong, 1993; Zhong and Mucci, 1995). Our main objective was to develop and appraise different thermodynamic equilibrium models for dilute Eu-calcite solid solutions and the coexisting aqueous solutions, to identify the substitution mechanisms involved in the incorporation of Eu(III) in calcite. Each model was tested against all three sets of experimental data.

1.4. Previous studies on REE Coprecipitation with Calcite

Experimental studies of trace REE partitioning in calcite were carried out by Terakado and Masuda (1988), Zhong (1993) and Zhong and Mucci (1995). Their results always indicated strong fractionation of REE(III) in calcite, with partition coefficients on the order of 10–1000 decreasing towards the heavy REEs. The partition coefficients measured by Terakado and Masuda (1988) are about one order of magnitude lower than those determined by Zhong and Mucci (1995), probably due to different coprecipitation techniques. The former authors used a free nucleation technique that commonly leads to partition coefficients below the equilibrium values for ions preferentially fractionating into the solid. This is a consequence of the high initial precipitation rates in such experiments (see e.g., Tesoriero and Pankow, 1996; Curti, 1999). The results of Zhong and Mucci (1995) appear to be more trustworthy, since they were obtained by means of a controlled slow precipitation technique. Being aware of the complications induced by the difference between the charge of Ca^{2+} and substituted ions, these authors proposed that the local charge balance for REE^{3+} incorporation is provided either by coupled substitution with Na^{+} or by vacant Ca^{2+} sites.

In another study, Carroll (1993) added relatively high Nd(III) concentrations ($10^{-5.5}$ to 10^{-4} M) to calcite suspensions, causing the precipitation of two new Nd-Ca phases. One of the precipitated phases was probably $Nd(OH)CO_3$, whereas the other fibrous precipitate remained unidentified. These Nd-Ca solids have little in common with the Eu-calcites considered in the present investigation, where added Eu concentrations were much lower ($m_{Eu} < 10^{-6}$ at pH 6 and 8, $m_{Eu} < 10^{-8}$ at pH 13.3).

In summary, most of the experimental data published so far do not form a basis for a thermodynamic analysis of heterovalent substitutions in calcite, since not all the information required for the application of solid solution models is provided. For instance, the total amount of added tracer should be varied systematically to construct isotherms, and precise measurements of mole fractions and equilibrium tracer concentrations in solution are needed. It is also essential to know precisely the amount of solid solution formed. Only the data published by Zhong (1993) and Lakshtanov and Stipp (2004) provide sufficient information and are therefore considered in our study.

2. MATERIALS AND METHODS

2.1. Recrystallization Experiments (pH 13)

2.1.1. Calcite

Powdered analytical grade calcite was purchased from Merck AG and used without further treatment. The average surface area from six replications was determined to be 0.31 $\pm$ 0.05 $m^2\ g^{-1}$ based on N_2 adsorption measurements (BET method) with a Micrometrics Gemini 2360 analyzer. The calcite composition was determined by ICP-AES and ICP-MS following dissolution of the calcite in 1 M HCl. K, Al and Eu were under the detection limit (0.1 ppb for Eu), whereas small impurities of Na (72 $\pm$ 4 ppm), Mg (65 $\pm$ 4 ppm) and Si (151 $\pm$ 7 ppm) were detected.

2.1.2. Artificial cement water

An artificial cement water (ACW) was used in all recrystallization tests. It is a highly alkaline (K, Na)OH solution saturated with portlandite and calcite (pH = 13.3). The ACW was prepared in a glove box under CO_2 exclusion by dissolving 11.9 g of KOH and 4.6 g of NaOH in 1 l of deionized water, and adding 1 g of $Ca(OH)_2$ (portlandite) and 1 g of $CaCO_3$ (calcite) to this solution. The ACW with the suspended solids was shaken for one week and filtered through a 0.1 μm Criticap^{TM} filter (Gelman Science) before it was used in the experiments.

Major element concentrations of the ACW solution, determined by ICP-AES, were, in mol/l: Na = 0.114 ± 0.002, K = 0.182 ± 0.006, Mg = (4.7 ± 0.4) × 10^{-7}, Ca = (1.6 ± 0.2) × 10^{-3}, Al = (3.7 ± 0.7) × 10^{-6}, Si = (6 ± 1) × 10^{-5}. Eu(III) concentrations, measured by ICP-MS, were found to be below the detection limit of 6.6 × 10^{-11} M.

2.1.3. Radiochemical and chemical analyses

Eu uptake was measured from solutions labeled with ^{152}Eu, whereas Ca uptake due to calcite recrystallization was determined from separate solutions spiked with ^{45}Ca. The ^{152}Eu source solution (37 MBq, from Amersham Pharmacia Biotech, Dübendorf, Switzerland) was diluted in 50 ml HCl (5%) to produce a stock solution. The ^{152}Eu / total Eu ratio was ~5% at the time of the experiments. Small aliquots (0.1–1 ml) of the stock solution were further diluted with 0.1 M HCl to obtain tracer solutions with the required total Eu initial concentrations (4 × 10^{-11} to 2 × 10^{-6} M). The ^{45}Ca source solution (37 MBq, from Isotopendienst Blasek GmbH, Waldburg, Germany) was diluted in 50 ml H_2O to produce a stock solution. Ten milliliters of the stock solution were further diluted with ACW to give a tracer solution with an activity of ~5000 Bq ml^{-1}. The ^{45}Ca / total Ca ratio of the tracer solution was ~0.04% at the time of the experiments.

^{152}Eu activities were measured on a Packard Minaxi 5530 gamma counter and a Packard Cobra 5003 auto gamma counter using the energy window between 15 keV and 400 keV. The background activity measured in this window for ^{152}Eu was typically ~150 cpm/5 ml. For very low ^{152}Eu activities a Canberra Packard Tri-Carb 2250CA liquid scintillation counter with an energy window between 6 keV and 70 keV was used. The background activity was typically ~30 cpm/5 ml. ^{45}Ca was measured on a Canberra Packard Tri-Carb 2250CA liquid scintillation counter using an energy window between 6 keV and 120 keV. The background activity measured in this window for ^{45}Ca was typically ~35 cpm/5 ml.

Element concentrations (Na, K, Ca, Al, Si, Eu) in the equilibrated solutions were determined by ICP-AES and ICP-MS. The pH stability of ACW-calcite suspensions was checked using a WTW Microprocessor 535 pH meter coupled either to Orion 8103 Ross combination pH electrodes or to Ingold combination pH electrodes.

2.1.4. Eu uptake experiments

All recrystallization experiments (including the ^{45}Ca exchange tests, see next section) were carried out in a glove box under a controlled N_2 atmosphere (O_2 and CO_2 concentrations <5 ppm) in 50 mL polyallomere centrifuge tubes that had been previously washed, left overnight in a solution of 0.1 M HNO_3 and finally rinsed with deionized water.

Calcite-ACW suspensions with a solid/water (S/W) ratio of 5 × 10^{-4} kg l^{-1} were prepared in polyethylene beakers, thoroughly mixed, homogenized with a shear mixer and equilibrated for approximately one hour with a magnetic stirrer. Aliquots (40 mL) were taken from the vigorously stirred suspensions and pipetted into 50 mL polyallomere centrifuge tubes. These samples were then spiked with 0.4 mL of the ^{152}Eu tracer solution and agitated on an end-over-end shaker for two weeks. The acid spike was added to the ACW solution after the calcite powder settled down to the bottom of the vials, so that the spike solution had time to homogenize with the ACW water before any contact with the calcite. The addition of a small amount of tracer solution (0.4 mL in 40 mL ACW) does not affect the final pH of the homogenized solution. Standards for the determination of total and specific activity of the tracer solutions were prepared by adding 0.4 ml aliquots of the ^{152}Eu tracer solution into counting vials and diluting them to 5 ml with ACW. After shaking, duplicate samples were taken from the vigorously stirred suspension to determine the total activity. After two weeks of equilibration, the solid and solution were separated by centrifugation of the suspensions for 1 h at 95 000 g (max.). Duplicate samples of the supernatant solution and samples previously withdrawn from the mixed suspensions were analyzed together with the standards. Finally, the pH was checked at the end of each adsorption test.

2.1.5. ^{45}Ca uptake experiments

Calcite suspensions with S/W ratios between 10^{-3} and 5 × 10^{-2} kg l^{-1} were prepared in polyethylene beakers by mixing the Merck calcite with 985 ml of ACW followed by the addition of 15 ml of the ^{45}Ca tracer solution. Standards for the determination of total and specific activity of the tracer solutions were prepared by adding 0.4 ml aliquots of the radionuclide tracer solution into counting vials and diluting them to 5 ml with ACW. Forty milliliter aliquots taken from the vigorously stirred suspensions were pipetted into 50 ml polyallomere centrifuge tubes and shaken on an end-over-end shaker for the desired equilibration time. After shaking, duplicate samples were taken from the vigorously stirred suspension to determine the total activity. After the desired reaction time, the solid and solution were separated by centrifugation for one hour at 95 000 g (max.). Duplicate samples from the supernatant solution and from the mixed suspensions were then analyzed with the gamma counter together with the standards.

2.2. Thermodynamic Calculations

2.2.1. Gibbs energy minimization

The Gibbs Energy Minimization (GEM) is a numerical method that has been applied to model thermodynamic equilibrium in a large variety of chemical systems. The main algorithm determines the global minimum of the total Gibbs free energy of a multiphase, multicomponent chemical system (Karpov et al., 1997; Karpov et al., 2001). This method is an alternative to the widespread Law of Mass Action (LMA) speciation models, formalized in various geochemical codes such as PHREEQC (Parkhurst and Appelo, 1999). In this investigation the GEM method (implemented in the GEM-Selektor code) was preferred to the LMA because of its suitability for solving complex solid solution equilibria. Furthermore, and in contrast to LMA codes, which can handle only one multicomponent phase (usually the aqueous solution), GEM codes allow an unlimited number of such phases to be included in the overall mass balance. It is therefore easy to solve equilibrium problems with complex multicomponent solid solutions, without the need for supporting tools such as Lippmann's functions (Glynn, 1991).

The stability of the j-th chemical species (dependent component, from the set L) at T, p of interest is defined by its standard chemical potential, μ_j^o (identical with its molar Gibbs free energy, G_j^o, taken from the input database). The equilibrium state is computed with GEM by determining the amounts of stable phases through a vector of mole amounts of dependent components $x = \{x_j,\ j \in L\}$ such that:

$$G(x) \Rightarrow \min, \quad \text{and} \quad Ax = b \tag{1}$$

where $A = \{a_{ij},\ i \in N,\ j \in L\}$ is a matrix defining the formula stoichiometry coefficients of dependent components; $b = \{b_i,\ i \in N\}$ is the input vector of mole amounts of independent components (from the set N of chemical elements and charge), and $G(x)$ is the total Gibbs energy function of the whole system:

$$G(x) = \sum_j x_j \mu_j,\ j \in L \tag{2}$$

In Equation 2, μ_j is a numerical approximation of the chemical potential of the j-th dependent component. The GEM-Selektor code works for convenience with normalized (dimensionless) chemical potentials, defined as:

$$\upsilon_j = \upsilon_j^o + \ln C_j + \ln \gamma_j + const, j \in L \tag{3}$$

where υ_j^o is the normalized (dimensionless) standard chemical potential, $C_j = f(x_j)$ is the species concentration, γ_j is the activity coefficient of the j-th species in a specific phase, and $const$ is a scaling factor that depends on the choice of the standard state ($const$ = ln 55.5084 for aqueous species, $const$ = ln p for gases and $const$ = 0 for solid solutions). Full expressions for υ_j in aqueous, gaseous, solid/liquid and adsorption phases are given by Karpov et al. (2001) and Kulik (2002).

The "Interior Points Method" (IPM) non-linear minimization algorithm—the "engine" of Selektor modeling codes—solves the problem posed through Eqn. (1) by finding simultaneously two vectors: the primal x and the dual u solutions. The vectors x and u must satisfy the *Karpov-Kuhn-Tucker* duality conditions (Karpov et al., 1997), which are necessary and sufficient to solve the chemical equilibrium problem, and in the simplest vector-matrix form can be written as:

$$\upsilon - A^T u \geq 0;$$
$$A\hat{x} = b;\ \hat{x} \geq 0;$$
$$\hat{x}^T(\upsilon - A^T u) = 0 \quad (4)$$

where ^{T} is the transpose operator. The vector u—the dual GEM solution—contains the normalized chemical potentials of independent components at equilibrium, u_j. The first condition in (Eqn. 4), rewritten with indices, states that for any j-th species present at equilibrium, the "primal" chemical potential υ_j (calculated from the equilibrium mole amount $\hat{x}_j$ and the normalized standard chemical potential υ_j^o, see Eqn. 3) must equal the "dual" chemical potential:

$$\upsilon_j = \sum_i a_{ij} u_i, j \in L, i \in N \quad (5)$$

The second condition represents mass balance constraints for total amounts of independent components, b_j. Finally, the last condition (of orthogonality) ensures that the mole amounts of unstable species and phases, to which the inequality in the first condition refers, are all set to zero.

All aforementioned calculations are implemented in the GEM-Selektor v.2-PSI code that uses the built-in, fully documented "Nagra/PSI 01-01" chemical thermodynamic database (Hummel et al., 2002). Both are available for download at http://les.web.psi.ch/Software/GEMS-PSI, and were used in modeling calculations for the present contribution.

2.2.2. *Dual thermodynamic calculations*

For any species in any phase at equilibrium, the first Karpov-Kuhn-Tucker condition Eqn. (4) can be combined with Eqns. (3) and (5) into a generic "dual thermodynamic equation" that relates primal and dual normalized chemical potentials:

$$\sum_i a_{ij} u_i = \frac{G^o_{j,T}}{RT} + \ln C_j + \ln \gamma_j + const \quad (6)$$

For the "inverse" modeling in the present contribution, Eqn. (6) provides the basis for "dual-thermodynamic" (DualTh) calculations—an efficient method to determine thermodynamic properties from the results of partitioning experiments (Kulik et al., 2000; Karpov et al., 2001; Kulik and Kersten, 2002). The basic idea of DualTh calculations is that, for any selected species j, one unknown parameter on the right side of Eqn. (6) can be determined if the others are known. For instance, (i) if the equilibrium composition of the aqueous solution and the mole fractions ($C_j = \chi_j$) of end-members in the coexisting solid solution are known, and assumptions can be made on the activity coefficients in the solid (e.g., $\gamma_j = 1$ for ideal solid solutions) then the molar Gibbs free energy of formation of the end-members can be derived. Alternatively, (ii) if the end-members and their Gibbs free energy of formation are known, Eqn. (6) can be used to determine activity coefficients in the solid. Because the chemical potential of any given independent component (u_i) must be the same in all equilibrated phases, the potentials can be determined independently by solving the GEM equilibrium problem only for the aqueous solution, without including any solid solution in the equilibrium calculations.

In our investigation, we applied both variants of the DualTh method to the calcite solid solutions formed in the previously mentioned recrystallization and coprecipitation experiments, assuming ideal mixing (see section 4). Note, however, that for variant (i), the assumption of ideality is just a matter of convenience. The Eu-calcites may well be non-ideal solid solutions, as it is impossible to determine simultaneously $G^o_{j,T}$ and γ_j from Eqn. (6), if stoichiometry and stability of the Eu end-members are not known independently. In such cases, the derived free energies of formation of the candidate end-members actually embed the activity coefficients. In other words, the following quantity can be determined from Eqn. (6):

$$G^*_{Eu-em} \equiv G^o_{Eu-em} + RT \ln \gamma_{Eu-em} = RT\left(\sum_i a_{ij} u_i - \ln \chi_{Eu-em}\right), \quad (7)$$

where χ_{Eu-em} (C_j in Eqn. 6) is the experimentally known mole fraction of the trace Eu end-member in the calcite solid solution, γ_{Eu-em} the corresponding activity coefficient (taken independent of χ_{Eu-em} at trace mole fractions of Eu end-member), and G^O_{Eu-em} the standard molar Gibbs free energy of the Eu end-member.

An important prerequisite for the applicability of Eqn. (7) is the constancy of the activity coefficients, i.e., the G^*_{Eu-em} values from different data points are comparable only if Henry's law applies. Since the great majority of Eu-calcites considered in our data analysis are dilute ($\chi_{Eu} < 0.01$), this condition is fulfilled.

Table 1. Recrystallization rates (mol m^{-2} s^{-1}) calculated from ^{45}Ca uptake experiments.

Step	10 g l^{-1}	50 g l^{-1}
0–11 days	$2.0 \pm 0.5 \times 10^{-11}$	$5.2 \pm 0.3 \times 10^{-11}$
11–90 days	$3.2 \pm 0.5 \times 10^{-12}$	$9.2 \pm 1.4 \times 10^{-12}$

3. RESULTS OF WET CHEMICAL EXPERIMENTS

3.1. ^{45}Ca Exchange in the Presence of Calcite at pH 13

Ca uptake experiments were carried out with a ^{45}Ca tracer, as described in section 2.1.5. The removal of ^{45}Ca from aqueous solution is a measure of the amount of recrystallized calcite, defining the mass of Eu-bearing solid solution at a given reaction time. This information is necessary for the calculation of Eu mole fractions (see section 3.2.1). Details on the evaluation of these data are given in Appendix 1.

The results of the ^{45}Ca experiments are reported in Table 1 and Figure 1, where the surface-normalized amounts of recrystallized calcite, calculated according to Eqn. (A1.2), are plotted as a function of reaction time. The data reveal a two-step kinetics and dependency on the solid/water (S/W) ratio. For both kinetic steps, the recrystallization rate measured at S/W = 50 g l^{-1} is about three times higher than at 10 g l^{-1}.

3.2. Recrystallization Experiments in the Presence of Eu Tracer

3.2.1. *Calculation of Eu mole fractions*

Eu mole fractions were calculated by dividing the amount of ^{152}Eu removed from solution by the amount, n [mol], of calcite recrystallized:

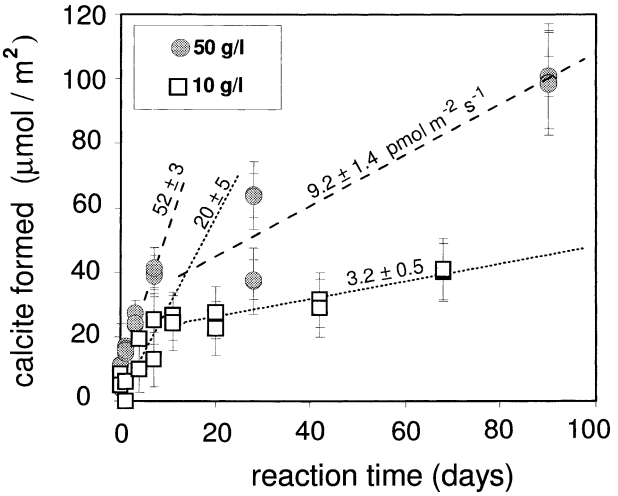

Fig. 1. Amounts of calcite formed and recrystallization rates derived from ^{45}Ca uptake experiments for calcite interacting with artificial cement pore water (pH 13.3).

Table 2. Initial and final Eu-molalities in ACW solution (m^{o}_{Eu} and m_{Eu}, respectively), and calculated Eu cationic mole fractions in the recrystallized calcite (χ_{Eu}).

	exp. ID	log (m^{o}_{Eu})	log (m_{Eu})	log (χ_{Eu})	u_{Eu}
exp. #1	1	−10.20	−11.79	−5.63	−337.4
	2	−9.69	−11.54	−5.12	−336.8
	3	−9.29	−11.33	−4.72	−336.3
	4	−8.72	−10.89	−4.15	−335.3
	5	−8.38	−10.41	−3.80	−334.2
	6	−8.09	−10.25	−3.52	−333.8
	7	−7.68	−9.77	−3.10	−332.7
	8	−7.17	−9.38	−2.59	−331.8
	9	−6.37	−8.73	−1.79	−330.3
	10	−5.74	−7.72	−1.17	−328.2
exp. #2	15	−10.39	−11.98	−5.83	−337.8
	14	−9.71	−11.26	−5.14	−336.2
	13	−9.27	−10.83	−4.70	−335.2
	12	−8.65	−10.27	−4.08	−333.9
	11	−8.16	−9.66	−3.60	−332.5

The rightmost column (u_{Eu}) gives the normalized (dimensionless) chemical potentials of Eu calculated with GEM-Selektor. The resulting u-values for major elements are: −121.1 (Na), −172.4 (C), −8.5 (O), −43.6 (H), −257.7 (Ca) and −128.9 (K).

$$\chi_{Eu} = \frac{W(m^{o}_{Eu} - m_{Eu})}{n} \quad (8)$$

where m^{o}_{Eu}, m_{Eu} are the initial and the final Eu tracer molalities, respectively, and W is the mass of water solvent. Note that Eqn. (8) defines empiric cationic mole fractions, representing the net fraction of octahedral sites occupied by Eu^{3+} ions. This definition implicitly assumes that *all* sites normally occupied by Ca^{2+} can be replaced by Eu^{3+} ions but in some cases this definition conflicts with thermodynamic principles. For instance, a cationic mole fraction of 2/3 would result for the pure $Eu_2\square(CO_3)_3$ defective structure, although the mole fraction of a pure solid end-member must be, by definition, equal to unity. In such cases, the cationic mole fractions must be rescaled for thermodynamic calculations.

3.2.2. *Presentation of results and uncertainties*

Results of the calcite recrystallization experiments in the presence of ^{152}Eu are listed in Table 2 as two separate isotherms (exp. #1 and exp. #2) and plotted in Figure 2, together with the results of the coprecipitation experiments of Lakshtanov and Stipp (2004) at pH 6 and those of Zhong (1993) at pH 8 that are reproduced in Tables 3 and Table 4, respectively. The data are shown in a logarithmic plot of equilibrium Eu molalities vs. Eu cationic mole fractions (thereafter referred as "isotherm-plot"), which is suitable for the thermodynamic analysis carried out in section 4. The following preliminary observations can be made: (i) the data obtained at pH 13 and pH 6 define a linear trend with a slope close to unity (0.90 ± 0.04 for exp. #1, 1.02 ± 0.03 for exp. #2 at pH 13, and 0.97 ± 0.06 for the coprecipitation experiments at pH 6); (ii) equilibrium Eu molalities for the recrystallization experiments are 1–2 orders of magnitude smaller than those measured by Lakshtanov and Stipp (2004) and ~3 orders of magnitude smaller than those of Zhong (1993). As discussed in section 4, the slope is a characteristic signature of the solid solution and puts constraints on the possible stoichiometries of the minor end-member.

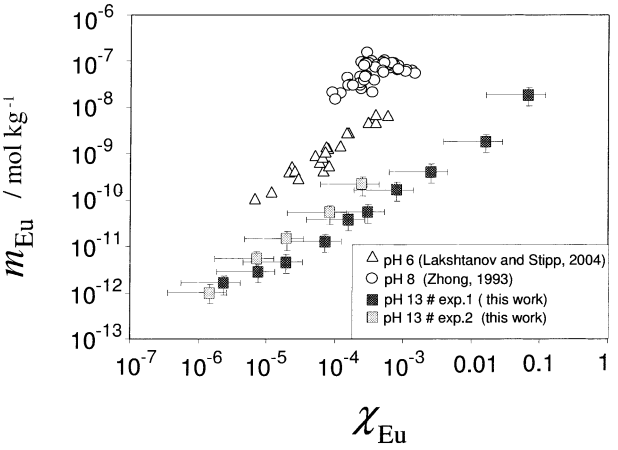

Fig. 2. Total Eu molalities as a function of Eu cationic mole fractions in calcite from three different studies. Analytical uncertainties are available only for the recrystallization tests.

For the experiments at pH ~13, the uncertainties of Eu equilibrium concentrations critically depend on the residual ^{152}Eu activity in the centrifuged supernatant. Due to the very strong Eu uptake in the solid phase, S/W ratios had to be optimized in such a way that a sufficiently high Eu activity remained in solution, while the mole fractions could still be determined with sufficient precision. The optimal S/W ratio was found to be ~0.5 g l^{-1}, giving an uncertainty of ± 44% on m_{Eu}. This is also the main reason for the different S/W ratios selected for the ^{45}Ca and ^{152}Eu experiments. Details on the determination of m_{Eu} uncertainties are given in Tits et al. (2002), Appendix A.

Mole fraction uncertainties were calculated from simple error propagation formulae applied to Eqn. (8), as described in section 4 of Bevington (1969). It was found that the main source of uncertainty is the ±76% uncertainty in the determination of the amount of recrystallized calcite, n, whereas other sources can be neglected. Therefore, all mole fractions have been assigned the same uncertainty of ±76%.

4. THERMODYNAMIC INTERPRETATION

4.1. Methodology

4.1.1. *On the issue of thermodynamic equilibrium*

A prerequisite for the successful application of chemical thermodynamics is the availability of experimental data for systems where phases and species under consideration are in mutual equilibrium. In the case of our recrystallization experiments, the primary (Eu-free) calcite is not part of the equilibrium system as it dissolves irreversibly. Equilibrium is assumed only between the aqueous solution and the recrystallized (Eu-bearing) calcite and, in the case of coprecipitation, between the aqueous solution and the precipitated calcite overgrowth, whereas the calcite seeds initially present are considered to remain inert. The constant addition method ensures the formation of compositionally homogeneous overgrowths.

Table 3. Initial and final Eu molalities in ACW solution (m^{o}_{Eu} and m_{Eu}, respectively), and calculated Eu cationic mole fractions (χ_{Eu}) in calcite overgrowths precipitated at pH 6 with the technique described by Tesoriero and Pankow (1996).

exp. #	log (m^{o}_{Eu})	log (m_{Eu})	log (χ_{Eu})	u_{Eu}	u_{Na}	u_{C}	u_{O}	u_{H}	u_{Ca}
3n	−5.79	−9.37	−4.17	−345.7	−138.4	−139.9	−9.6	−43.0	−286.8
4n	−6.80	−9.96	−5.18	−347.7	−138.4	−140.9	−9.1	−43.3	−287.3
5n	−5.72	−9.26	−4.10	−346.0	−138.3	−140.7	−9.2	−43.2	−287.2
6n	−5.91	−9.03	−4.29	−345.5	−138.4	−140.8	−9.1	−43.3	−287.3
7n	−6.54	−9.82	−4.94	−347.3	−138.4	−140.8	−9.2	−43.3	−287.3
8s	−5.92	−9.27	−4.64	−345.9	−137.6	−140.5	−9.3	−43.2	−287.1
9s	−5.96	−9.39	−4.68	−346.2	−137.7	−140.6	−9.3	−43.2	−287.1
10n	−5.82	−9.18	−4.23	−346.0	−138.4	−141.0	−9.1	−43.3	−287.3
11n	−5.52	−8.82	−3.92	−345.3	−138.5	−141.2	−9.0	−43.4	−287.4
12s	−4.82	−8.18	−3.23	−344.0	−138.5	−141.4	−8.9	−43.4	−287.6
13s	−5.89	−9.37	−4.60	−346.0	−137.4	−140.4	−9.4	−43.2	−287.0
14s	−5.49	−9.08	−4.19	−345.4	−137.5	−140.5	−9.3	−43.2	−287.1
15s	−5.10	−8.54	−3.80	−344.1	−137.5	−140.3	−9.4	−43.2	−287.0
16s	−5.40	−8.89	−4.10	−345.0	−137.6	−140.5	−9.3	−43.2	−287.1
17s	−4.82	−8.32	−3.53	−343.6	−137.5	−140.3	−9.4	−43.2	−287.0
18s	−5.70	−8.85	−4.13	−345.6	−138.5	−141.5	−8.8	−43.4	−287.6
19s	−5.00	−8.33	−3.42	−344.5	−138.5	−141.5	−8.8	−43.4	−287.6
20s	−5.00	−8.16	−3.41	−344.1	−138.5	−141.5	−8.8	−43.5	−287.6
21s	−5.12	−8.96	−4.14	−344.1	−138.5	−141.5	−8.8	−43.5	−287.6
22s	−4.82	−8.55	−3.83	−344.1	−138.5	−141.5	−8.8	−43.5	−287.6
23s	−5.53	−9.53	−4.54	−344.1	−138.5	−141.5	−8.8	−43.5	−287.6

The experimental data (m^{o}_{Eu} and m_{Eu}) were kindly supplied by Lakshtanov and Stipp (2004). The table also shows the normalized (dimensionless) chemical potentials of Eu and other elements, calculated with GEM-Selektor (this work).

Thorstenson and Plummer (1977) introduced the concept of "stoichiometric saturation" to describe the pseudoequilibrium state reached upon the congruent dissolution of Mg-calcites. This phenomenon is common for metastable phases dissolved at low temperatures and is frequently observed when calcite solid solutions dissolve (Gamsjäger 1985). In contrast, when carbonate solid solutions *precipitate* from an oversaturated solution or recrystallize, the incorporation of foreign ions is not stoichiometric, unless the partition coefficient is equal to 1 (Glynn et al., 1990). At sufficiently low precipitation rates, the composition of the newly formed solid approaches equilibrium with the solution. Gamsjäger (1985) and Gamsjäger et al. (2000) discussed several binary systems and concluded that in most dissolution experiments, especially over relatively short reaction times, stoichiometric saturation was observed, whereas in precipitation experiments (e.g., Mucci and Morse, 1984) the data plot close to the solidus and solutus curves on a Lippmann diagram. From this it is concluded that experiments carried out from the oversaturation-side, especially at the slowest precipitation rates, tend to approach thermodynamic equilibrium. Since all experiments selected for this study were carried out at calcite growth rates where empiric partition coefficients are insensitive to precipitation kinetics, it seems justified to

Table 4. Initial and final Eu molalities in ACW solution (m^{o}_{Eu} and m_{Eu}, respectively), and calculated Eu cationic mole fractions (χ_{Eu}) for calcites coprecipitated in artificial seawater at pH 8 (data from Zhong, 1993).

exp. #	log (m^{o}_{Eu})	log (m_{Eu})	log (χ_{Eu})	u_{Eu}	u_{Na}	u_{C}	u_{Ca}
sz-113	−7.51	−7.59	−3.63	−344.7	−136.0	−163.5	−287.6
sz-114	−7.45	−7.51	−3.65	−344.7	−136.0	−163.5	−287.6
sz-115	−7.60	−7.67	−3.47	−345.1	−136.1	−163.4	−287.7
sz-116	−7.68	−7.76	−3.99	−345.6	−136.2	−163.3	−288.0
sz-117	−7.30	−7.33	−3.65	−344.3	−136.1	−163.4	−287.7
sz-118	−7.32	−7.35	−3.83	−344.3	−136.1	−163.4	−287.7
sz-122	−7.45	−7.51	−3.75	−344.9	−136.2	−163.3	−287.9
sz-123	−7.45	−7.50	−3.79	−344.6	−136.1	−163.5	−287.7
sz-124	−7.47	−7.52	−3.82	−344.7	−136.1	−163.4	−287.7
sz-126	−7.64	−7.67	−4.05	−345.8	−136.4	−163.1	−288.4
sz-127	−7.76	−7.81	−4.01	−345.6	−136.2	−163.3	−287.9
sz-199	−7.27	−7.41	−3.59	−344.7	−136.3	−163.3	−288.1
sz-202	−7.13	−7.23	−3.30	−344.4	−136.2	−163.4	−288.0
hs-205	−7.23	−7.30	−3.56	−344.5	−136.2	−163.4	−288.1
hs-206	−7.29	−7.40	−3.44	−344.8	−136.3	−163.3	−288.3
hs-208	−7.27	−7.33	−3.57	−344.6	−136.3	−163.3	−288.2

The table also shows the normalized (dimensionless) chemical potentials of Eu and other elements calculated with GEM-Selektor (this work). The potentials of oxygen and hydrogen have constant values throughout all experiments ($u_O = -0.78$ and $u_H = -47.5$). Only data points with Eu concentrations below the solubility of $EuOHCO_3$ (cr) were considered. For all the listed data, log (pCO_2, bar) = -2.5 ± 0.1.

Table 5. Selected end-members used in the forward modeling of Eu-calcite solid solutions, with the measured solubility products of corresponding pure crystalline Eu phases.

Eu end-member	Ca end-member	Assumed substitutions	log K^{o}_{sp} (Eu end-member)	source
$Eu_2(CO_3)_3$	$Ca_3(CO_3)_3$	$2\ Eu^{3+} \rightleftharpoons 3\ Ca^{2+}$	-35.0 ± 0.3	1,2
$NaEu(CO_3)_2$	$Ca_2(CO_3)_2$	$Eu^{3+} + Na^{+} \rightleftharpoons 2\ Ca^{2+}$	-20.5 ± 0.7	3,4
$EuOHCO_3$	$CaCO_3$	$EuOH^{2+} \rightleftharpoons Ca^{2+}$	-21.7 ± 0.1	1,2
$Eu(OH)_3$	$CaCO_3$	$Eu^{3+} + 3\ OH^{-} \rightleftharpoons Ca^{2+} + CO_3^{2-}$	-27.1 ± 0.3	1,5

[1](Hummel et al., 2002); [2](Runde et al., 1992); [3](Fannin, 1999); [4](Fannin et al., 2002); [5] (Bernkopf, 1984).

assume that Eu equilibrium partitioning was approached to an extent sufficient to apply equilibrium thermodynamics.

4.1.2. Modeling approach

As discussed in section 1.2, the identification of the minor end-member is not straightforward for heterovalent solid solutions, due to local charge balance requirements and non-isomorphic substitution. From the point of view of thermodynamics, there are no limitations in the selection of possible stoichiometries, as long as the experimental partitioning data can be described correctly. Nevertheless, the selected end-member should be compatible with simple crystal-chemical and mineralogical criteria. For instance, the host structure may have a limited tolerance to lattice deformation, or lack suitable interstitial sites to accommodate large substituents. In this respect, a careful review of known mineral structures, in which the trace element under consideration occurs as a major ion, may be helpful in identifying the stoichiometry and structure of non-isomorphic minor end-members.

Two strategies were followed to model the experimental data. The first one ("forward" modeling) involved the direct calculation of ideal solid solution models for the specific conditions of the selected experiments, using as minor end-members pure Eu solids with known solubility products (Table 5). For each end-member pair and each of the three available datasets, equilibrium Eu solution concentrations and mole fractions in the solid were predicted from GEM calculations across the compositional range of interest ($m^{o}_{Eu} = \sim 10^{-11} - 10^{-5}$ mol kg^{-1}) and then compared with the experimental data. The advantage of this method is that model parameters and experimental data are independent of each other, because the relevant thermodynamic properties (i.e., solubility product) of the postulated Eu end-member have been determined experimentally.

Conversely, the forward modeling method is not applicable to end-members for which no solubility or free energy data are available. In such cases, we resorted to an alternative approach, called here "inverse" modeling. The theoretical background of this method is explained in section 2.2 and a practical application is described later in section 4.3. This technique has already been applied to model solid solution formation in cement systems (Kulik and Kersten, 2002) and marine carbonates (Kulik et al., 2000).

With the inverse modeling approach, the free energy of formation of the proposed end-member is determined through DualTh calculations directly from the experimental partitioning data, under the assumption that the measured solution concentrations and mole fractions in the solid solution reflect equilibrium. Note that it is not necessary to include the solid solution explicitly in such DualTh calculations, because chemical potentials are equal for all thermodynamic phases in mutual equilibrium. In other words, the derivation of chemical potentials of independent components in the equilibrated aqueous solution directly yields the corresponding chemical potentials in the solid solution. An additional assumption made in our model is that the solid solutions are either ideal or that Henry's law applies (constant activity coefficient of the minor component in the case of non-ideality). For most binary solid solutions, Henry's law applies at $\chi < 0.01$, a condition fulfilled by all but two of the data points considered in this study (see Fig. 2). The reasons for making this assumption are explained in section 4.3.

4.2. Predictions from End-Members with Known Solubility (Forward Modeling)

Solubility products are known for the crystalline Eu compounds $Eu_2(CO_3)_3$, $NaEu(CO_3)_2.6H_2O$, $EuOHCO_3$ and $Eu(OH)_3$. Accordingly, forward modeling could be applied only to these four end-member stoichiometries. The solubility products of the mentioned solids are listed in Table 5, together with the corresponding Ca end-members and the implied substitution mechanisms.

The predicted isotherms are plotted in Figures 3, 4 and 5, where they are compared with the corresponding experimental data (see Fig. 2). All calculations were carried out with the GEM-Selektor code at 25°C and 1 bar total pressure, using the thermodynamic constants specified in Hummel et al. (2002) and applying Davies' equation (with coefficient 0.3) for the calculation of aqueous ion activity coefficients. The gas phase was modeled as a mixture of ideal gases. In Table 6, typical speciation results are listed for each of the three datasets, whereas in Figure 6, the distribution of Eu species is plotted as a function of pH to reproduce approximately the solution compositions of the three studies considered in this paper.

Note that for the coprecipitation data of Zhong (1993), chemical equilibrium calculations were carried out assuming the actual average saturation index (SI = log $\Omega \sim 0.8$, where Ω is the extent of oversaturation). Since the solution data of Lakshtanov and Stipp (2004) suggest that calcite precipitation occurred close to equilibrium (SI <0.3), for these experiments, as for the recrystallization experiments, our calculations were carried out assuming exact saturation conditions.

The model calculations yielded isotherms with characteristic slopes (+1/2 for the $Eu_2(CO_3)_3$ end-member and of + 1 for the other three end-members). In Appendix 2 we demonstrate that, for dilute solid solutions, the isotherm slope is a fingerprint of

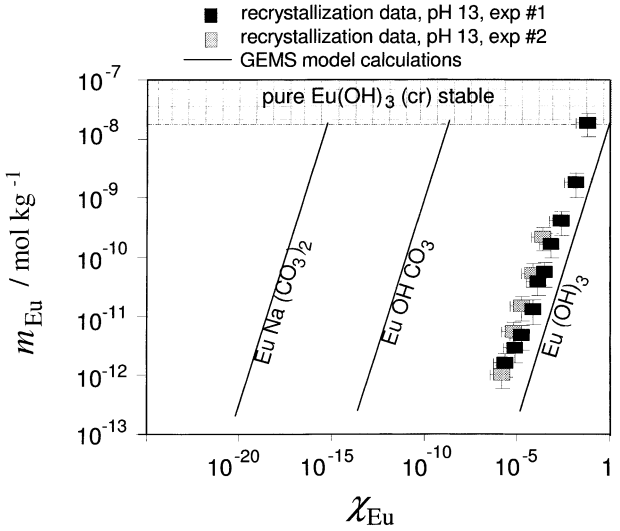

Fig. 3. Comparison of binary ideal solid solution models (GEM calculations) with Eu uptake data from recrystallization experiments carried out in ACW water (pH 13). Each line represents a model for one of the end-member pairs defined in Table 5. Calculations with the $Eu_2(CO)_3$ end-member predict total exclusion of Eu from the calcite lattice, yielding physically unreasonable mole fractions ($\chi_{Eu} < 10^{-25}$) that fall outside of the plot.

the assumed end-member stoichiometry and, thus, it gives some insight into the substitution mechanism. For instance, choosing $Eu_2(CO_3)_3$ as end-member implies the replacement of a $Ca_3(CO_3)_3$ group by a "dimeric" $Eu_2(CO_3)_3$ group. In all other cases, the stoichiometric coefficient associated to Eu in the end-member formula is one, meaning that Eu^{3+} ions are incorporated as isolated entities, so that each Eu^{3+} ion is surrounded only by Ca^{2+} ions in all adjacent octahedral positions. The different slopes arise ultimately from different entropies of mixing for the incorporation of "monomeric" and

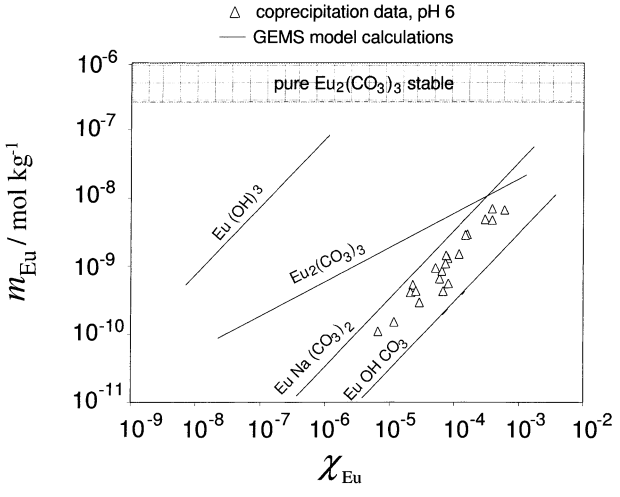

Fig. 4. Comparison of binary ideal solid solution models (GEM calculations) with Eu-calcite coprecipitation data from experiments carried out in a 0.025–0.1 m $NaClO_4$ medium (pH 6) by Lakshtanov and Stipp (2004). Each line represents a model for one of the end-member pairs defined in Table 5.

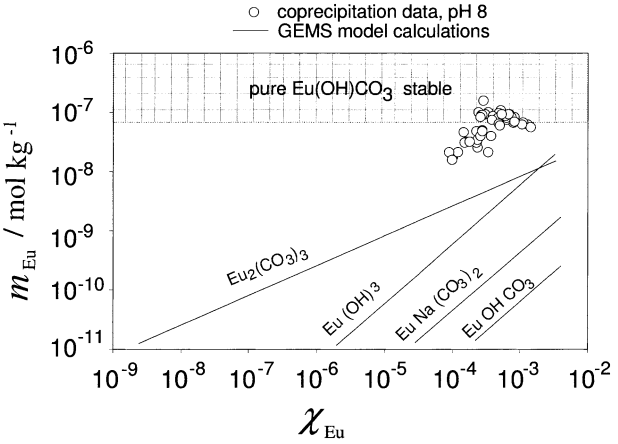

Fig. 5. Comparison of binary ideal solid solution models (GEM calculations) with Eu-calcite coprecipitation data from experiments carried out in artificial seawater (pH 8) by Zhong (1993). Each line represents a model for one of the end-member pairs defined in Table 5.

"polymeric" groups. As the isotherms (datasets at pH ~ 6 and pH ~ 13) exhibit a slope close to unity, incorporation of "dimeric" Eu-Eu pairs on adjacent octahedral sites must be ruled out, which forces us to reject the $Eu_2(CO_3)_3$ end-member.

Although the three remaining end-members produce an isotherm slope compatible with the experimental data, a closer analysis reveals that none of these models is able to reproduce simultaneously all measurements. For the recrystallization data at pH 13 (Fig. 3), only the $Eu(OH)_3$–$CaCO_3$ solid solution is compatible with the experimental results. The $NaEu(CO_3)_2$ and $Eu(OH)CO_3$ solid solution models require equilibrium mole fractions of less than 10^{-10}, implying nearly total Eu exclusion from calcite, a prediction that clearly disagrees with experimental observations. Consequently, due to the unreasonably large activity coefficients required to fit the data, also these end-members must be ruled out. For instance, given the nine orders of magnitude difference between measured Eu molalities and those predicted by the model based on the solubility product of crystalline $Eu(OH)CO_3$, a strongly negative Margules parameter ($a_0 = W_G/RT = -16.9$) would be required, a value that cannot be reconciled with any experimental value or empiric estimate. According to the compilation of Glynn (2000), a_0 values are mostly positive and never exceed a value of ~6 for carbonate solid solutions.

A quite different picture emerges when the forward modeling approach is applied to the coprecipitation experiments of Lakshtanov and Stipp (2004) (Fig. 4). The degree of non-ideality is in general smaller and the predictions based on the $EuNa(CO_3)_2$ as well as $EuOHCO_3$ end-members fall fairly close to the experimental data.

Specifically, the non-ideality correction for the $EuOHCO_3$-$CaCO_3$ solid solution would require a positive Margules parameter ($a_0 = W_G/RT \sim 2$) close to the values known for many binary sulfate and carbonate solid solutions, whereas for the coupled $Eu^{3+} + Na^+$ substitution mechanism, a negative parameter is necessary, which is rather unusual for carbonates (Glynn, 2000). The latter mechanism can also be excluded based on the insensitivity of measured Eu equilibrium concentrations to the Na concentration in solution, as noted by Lak-

Table 6. Typical solution speciation for the three types of experiments considered.

	pH 6	pH 8	pH 13
pH	6.4	7.9	13.3
Ionic Strength (mol kg^{-1})	0.114	0.661	0.280
log (pCO_2, bar)	0	−2.5	−13.2
Eu speciation (nanomol kg^{-1})			
Eu^{3+}	0.02	0.6	
$EuCO_3^+$	1.5	55	
$Eu(CO_3)_2^-$	0.06	45	
$EuOH^{2+}$		0.2	
$Eu(OH)_2^-$		0.2	
$Eu(OH)_3$ (aq)		0.02	1.6
$Eu(OH)_4^-$			14
$EuSO_4^+$		1.5	
Major species (millimol kg^{-1})			
Na^+	45.8	480.2	103.9
$NaHCO_3$ (aq)	0.7	0.6	
NaOH (aq)			10.4
$NaSO_4^-$		7.4	
K^+		10.0	173.4
KOH (aq)			0.9
KSO_4^-		0.2	
Ca^{2+}	21.2	8.9	0.5
$CaHCO_3^+$	4.7	0.1	
$Ca(OH)^+$			1.0
$Ca(OH)_2$ (aq)			0.1
$CaSO_4$ (aq)		1.7	
Mg^{2+}		44.5	
$MgCO_3$ (aq)		0.1	
$MgHCO_3^+$		0.6	
$MgSO_4$ (aq)		10.0	
Cl^-		565.7	
ClO_4^-	44.8		
HCO_3^-	48.2	3.8	
CO_3^{2-}	0.01	0.03	0.07
OH^-			279.1
SO_4^{2-}		9.9	
Br^-		0.9	

All calculations were performed for $T = 25°C$, $p = 1$ bar with the GEM-Selektor code, using Davies' equation for aqueous activity coefficients. Major aqueous species appear only if contributing more than 1 % of the element speciation.

shtanov and Stipp (2004). Finally, the $Eu(OH)_3$-$CaCO_3$ solid solution, the only suitable model to explain the recrystallization data at pH 1.3, must be ruled out as explanation of the pH 6 data, since it yields unreasonable predictions requiring exceedingly large non-ideality corrections.

The data of Zhong (1993) can be realistically described assuming binary mixtures with either the $Eu_2(CO_3)_3$ or $Eu(OH)_3$ end-member, whereas binary solid solutions with $EuNa(CO_3)_2$ or $Eu(OH)CO_3$ must be ruled out. Unfortunately, the limited Eu mole fraction range of their precipitates and their proximity to the $Eu(OH)CO_3$(cr) saturation limit (which seems to be exceeded in some cases) preclude the determination of the isotherm slope.

The general picture emerging from the forward modeling is that none of the four assumed binary solid solution models is capable to explain all three datasets. It appears that either (i) there are at least two distinct Eu coordination environments in calcite, depending on experimental conditions (pH from 6 to 13 and pCO_2 from ~ 0 to 1 bar), or (ii)—if we postulate a common coordination environment—we have to resort to alternative end-members.

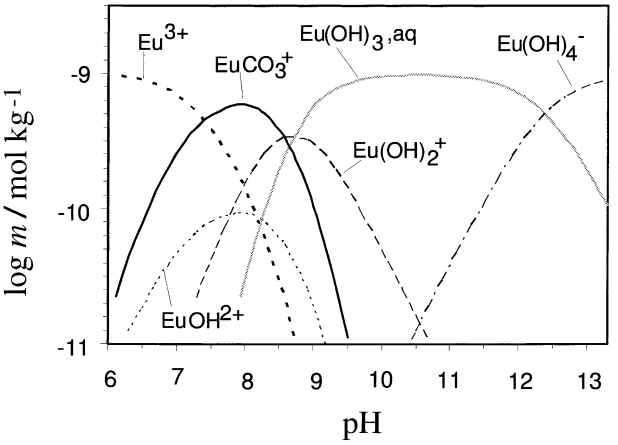

Fig. 6. Speciation in a 10^{-9} M $Eu(NO_3)_3$ + 0.1 m $NaClO_4$ solution as a function of pH at $T = 25°C$ and $p = 1$ bar (GEM calculations). The pH was varied through appropriate additions of carbonic acid or sodium hydroxide. No Eu sulfate complex appears at pH 8 (see Table 6), since these speciation calculations refer to a sulfate-free system. No equilibrium with a gas phase was assumed.

4.3. Inverse Modeling with Alternative End-Members

Selecting end-members with known solubility product is mainly a matter of convenience. Many alternative stoichiometries can be proposed, as suggested by the large variety of REE-carbonates that exist in nature (see e.g., Strunz and Nickel, 2001). It is not possible to test all conceivable stoichiometries and structural environments of Eu in calcite and thus we restricted our choice to the simplest ones, avoiding complex structural units that could not readily fit into the calcite lattice. In addition, we only considered stoichiometries that allow incorporation of isolated Eu^{3+} ions, in agreement with the slope of +1 defined by the data in the isotherm plots (Fig. 2).

Based on the criteria outlined above, the following alternative end-member pairs were selected for a test with the inverse method: $EuH(CO_3)_2$–$Ca_2(CO_3)_2$, $EuO(OH)$–$CaCO_3$ and $EuO(CO_3)_{0.5}$–$CaCO_3$. The first end-member pair represents a case of coupled substitution, $H^+ + Eu^{3+} = 2\ Ca^{2+}$, whereas for the second and third pairs Eu^{3+} is incorporated with "free" O^{2-} ions, i.e., hydroxyls or oxygens not belonging to carbonate groups.

In the first step, aqueous equilibria were computed with GEM-Selektor, yielding normalized chemical potentials of the dissolved elements assumed to be in equilibrium with the Eu-calcite solid solution. These DualTh calculations differ fundamentally from those performed with the forward modeling approach, because precipitation and dissolution of solid solution phases were explicitly excluded from the chemical calculations. Only the speciation and chemical potentials u_i of the elements in the aqueous solution were computed. The chemical potential of any given candidate end-member (indexed with α) was then simply derived from linear combinations of the ele-

mental potentials u_i and corresponding stoichiometric coefficients a_i: $\mu_\alpha \equiv RT\,\upsilon_\alpha = RT\,\Sigma\,(a_i\mu_i) = \Sigma\,(a_i\mu_i)$ (see Eqn. 5). For example, the chemical potential of the $EuNa(CO_3)_2$ end-member is obtained as:

$$\mu_{EuNa(CO_3)_2} = \mu_{Eu} + \mu_{Na} + 2\mu_C + 6\mu_o \quad (9)$$

In this way, the equilibrium potentials of all proposed alternative end-members were derived for each aqueous solution belonging to a given isotherm. For comparison, we also calculated the potentials of end-members previously used in the forward modeling approach (listed in Table 5).

In the second step of the DualTh inverse modeling procedure, the sum of the molar free energy of formation G^o_α and activity coefficient term $RT\ln\gamma_\alpha$ was calculated for each postulated end-member, with the help of the measured mole fractions. Applying Eqn. (7) to the example above yields:

$$G^*_{EuNa(CO_3)_2} = \mu_{EuNa(CO_3)_2} - RT\ln\chi_{EuNa(CO_3)_2} \quad (10)$$

The average and standard deviation of the G^*_α values resulting from the experimental points of a specific isotherm were then calculated separately for each end-member. Note that the (unknown) activity coefficient term in Eqn. (7) must be assumed to be constant to make the single G^*_α values comparable within the isotherm and to allow extension of the calculated statistical uncertainty to G^o_α. This important requirement is fulfilled because the great majority of the Eu-calcite solid solutions considered in our study are dilute (linear Henry's law region).

If a postulated end-member α is appropriate, identical G^*_α-values should result for all data points belonging to the same isotherm, whereas inappropriate end-members would yield large statistical variations. In practice, two criteria must be satisfied to confirm a potential end-member. First, the standard deviation of the mean G^*_α values resulting from all points on the isotherm should not exceed $\pm$ 2 kJ mol^{-1}, which corresponds to the commonly expected precision of $\pm$0.3 pK-units in solubility product measurements. The second criterion is that no trend should be present in the series of computed G^*_α-values. If the isotherm slope predicted for a given end-member pair differs from that defined by the experimental points, then the calculated G^*_α values will decrease or increase systematically as a function of mole fraction.

Note that solution oversaturation has no significant effect on the calculated free energies since, for a system at fixed pH and pCO_2, only the chemical potential of Ca is affected when the saturation state is varied. The elemental potentials of Eu, C, O, H, Na, on which the chemical potentials of the postulated dilute end-members depend, remain almost unaffected when the SI of calcite varies.

The results of DualTh calculations are shown in Table 7 and the related statistics are summarized in Table 8. The first observation is that, as expected from the results of the forward model, the largest standard deviations occur when $Eu_2(CO_3)_3$ is assumed as end-member. For the pH 6 and pH 13 data, the corresponding calculated G^*_α values vary systematically along the isotherms (see Table 7, where the data are listed in order of increasing Eu mole fractions). These trends simply reflect a discrepancy between predicted and observed slope in the isotherm plots. All other end-members yield acceptable statistics, with standard deviations of about $\pm$ 2 kJ mol^{-1}.

If the same Eu incorporation mechanism were operating in all three types of experiments, it should be possible to find an end-member pair yielding the same mean G^*-values for all three datasets. Inspection of Table 8 reveals that this is not the case. For each of the seven proposed end-member pairs, at least one of the three average G^*-values is discordant. On the other hand, the binary model involving $EuH(CO_3)_2$ as end-member yields (within the statistical uncertainty) coincident mean G^*-values for the pH 6 and pH 8 data, whereas the models involving EuO(OH) or $Eu(OH)_3$ yield coincident mean G^*-values for the pH 8 and pH 13 data.

To give a more pragmatic idea of the DualTh method, we converted the mean standard potentials into fictitious solubility products (Table 9) by first calculating the Gibbs free energy of the relevant dissolution reaction, $\Delta_R G^*$, then applying the fundamental relation $\Delta_R G^* = -RT\ln K^*_{sp}$. For all end-members, discrepancies of several orders of magnitude in the log K^*_{sp} values result at least for one of the three datasets. Consistent constants (outlined in bold) are derived for two of three datasets with the binary models involving $EuH(CO_3)_2$, EuO(OH) or $Eu(OH)_3$.

It is important to note here that, as long as water activity is close to unity, the EuO(OH) and $Eu(OH)_3$ end-members are thermodynamically equivalent, since the dissolution reactions differ only by the number of water molecules involved. Actually, a continuous series of equivalent end-members with the generic formula $EuO_{x/2}(OH)_{3-x}$, between the hydroxyl-free $EuO_{3/2}$ and the fully hydrated $Eu(OH)_3$ stoichiometries can be defined. Thus, it is not possible to infer the degree of hydration of the substituted Eu(III)-complex from the thermodynamic analysis alone. Remarkably, the solubility constants of 16.4 $\pm$ 0.2 and 16.2 $\pm$ 0.3 extrapolated from the DualTh calculations for the $Eu(OH)_3$ end-members are close to the experimental solubility products of $Eu(OH)_3$ and lie between the values determined for the amorphous and crystalline solids.

4.4. Modeling with a Ternary Solid Solution

The results described in the preceding sections indicate that the ensemble of available data on Eu-calcites cannot be modeled with a simple binary solid solution. On the other hand, the DualTh calculations indicate that binary solid solutions including the $EuH(CO_3)_2$ or a $EuO_{x/2}(OH)_{3-x}$ end-member successfully reproduce two of the three datasets. The next logical step was therefore to construct a ternary model involving the two latter end-members as Eu poles and $CaCO_3$ as the Ca pole.

Figure 7 shows the results obtained from forward GEM-Selektor calculations with the ideal ternary solid solution $EuH(CO_3)_2$–EuO(OH)–$CaCO_3$, assuming $G^*_{EuH(CO3)2} = -1773$ kJ mol^{-1} and $G^*_{EuO(OH)} = -955$ kJ mol^{-1}. These free energies, obtained by slightly adjusting the G^*-values of the two Eu components until the best simultaneous fit for the three sets of data were found, are close to those determined for the binary solid solutions (highlighted in bold in Table 8).

Figure 7 shows that this ternary model adequately reproduces all three datasets considered in this investigation. More importantly, any other ternary solid solution resulting from systematic combinations involving one or more of the $Eu_2(CO_3)_3$, $EuOH(CO_3)$, $EuNa(CO_3)_2$ and $EuO(CO_3)_{0.5}$ end-

Table 7. Free energies of formation, including activity correction term (G^*_α), for candidate Eu end-members at T = 25°C and p = 1 bar.

	G^*_α for candidate Eu end-members (kJ mol^{-1})						
Eu pole Ca pole	$Eu_2(CO_3)_3$ $Ca_3(CO_3)_3$	$EuOH(CO_3)$ $CaCO_3$	$EuNa(CO_3)_2$ $Ca_2(CO_3)_2$	$Eu(OH)_3$ $CaCO_3$	$EuH(CO_3)_2$ $Ca_2(CO_3)_2$	$EuO(OH)$ $CaCO_3$	$EuO(CO_3)_{0.5}$ $CaCO_3$
exp. ID	recrystallization experiments (pH 13), this work						
15	−3113.9	−1423.7	−2087.0	−1191.6	−1894.8	−954.4	−1070.4
1	−3112.8	−1423.7	−2087.0	−1191.6	−1894.8	−954.4	−1070.4
14	−3109.6	−1423.5	−2086.8	−1191.3	−1894.6	−954.1	−1070.2
2	−3112.9	−1425.2	−2088.5	−1193.1	−1896.3	−955.9	−1072.0
3	−3112.8	−1426.4	−2089.6	−1194.2	−1897.4	−957.0	−1073.1
13	−3107.2	−1423.6	−2086.9	−1191.4	−1894.7	−954.2	−1070.3
4	−3111.0	−1427.1	−2090.4	−1194.9	−1898.2	−957.7	−1073.8
12	−3104.3	−1423.9	−2087.2	−1191.8	−1895.0	−954.5	−1070.6
5	−3107.5	−1426.3	−2089.6	−1194.1	−1897.4	−956.9	−1073.0
11	−3100.0	−1423.2	−2086.5	−1191.0	−1894.3	−953.8	−1069.9
6	−3107.4	−1427.1	−2090.3	−1194.9	−1898.1	−957.7	−1073.8
7	−3104.2	−1426.7	−2090.0	−1194.5	−1897.8	−957.3	−1073.4
8	−3102.7	−1427.4	−2090.6	−1195.2	−1898.4	−958.0	−1074.1
9	−3099.8	−1428.2	−2091.5	−1196.0	−1899.3	−958.8	−1074.9
10	−3092.8	−1426.5	−2089.8	−1194.3	−1897.6	−957.1	−1073.2
	coprecipitation experiments (pH 6), from Lakshtanov and Stipp (2004)						
12s	−2937.3	−1380.3	−2012.1	−1223.1	−1776.4	−985.9	−1064.5
20s	−2935.9	−1379.1	−2010.7	−1221.9	−1775.2	−984.7	−1063.3
19s	−2937.8	−1380.1	−2011.7	−1222.9	−1776.2	−985.7	−1064.3
17s	−2937.5	−1379.6	−2009.7	−1222.4	−1775.7	−985.2	−1063.8
15s	−2938.2	−1379.2	−2009.1	−1222.0	−1775.3	−984.8	−1063.4
22s	−2933.5	−1376.7	−2008.3	−1219.5	−1772.8	−982.3	−1060.9
11n	−2940.7	−1380.0	−2012.0	−1222.8	−1776.1	−985.6	−1064.2
5n	−2944.6	−1381.5	−2013.4	−1224.3	−1777.6	−987.1	−1065.7
16s	−2940.5	−1379.4	−2009.5	−1222.2	−1775.6	−985.1	−1063.7
18s	−2939.7	−1379.0	−2010.7	−1221.8	−1775.1	−984.6	−1063.2
21s	−2931.7	−1374.9	−2006.6	−1217.7	−1771.1	−980.6	−1059.2
3n	−2945.4	−1381.7	−2014.2	−1224.5	−1777.8	−987.3	−1065.9
14s	−2942.1	−1380.0	−2009.9	−1222.8	−1776.1	−985.6	−1064.2
10n	−2942.9	−1380.3	−2012.1	−1223.0	−1776.4	−985.9	−1064.5
6n	−2940.8	−1379.1	−2010.9	−1221.9	−1775.2	−984.7	−1063.3
23s	−2929.4	−1372.6	−2004.3	−1215.4	−1768.8	−978.2	−1056.9
13s	−2943.0	−1379.3	−2009.1	−1222.1	−1775.4	−984.9	−1063.5
8s	−2941.8	−1378.5	−2008.7	−1221.3	−1774.6	−984.1	−1062.7
9s	−2942.8	−1379.0	−2009.2	−1221.8	−1775.1	−984.6	−1063.2
7n	−2946.2	−1379.9	−2011.7	−1222.7	−1776.0	−985.5	−1064.1
4n	−2946.4	−1379.3	−2011.2	−1222.1	−1775.4	−984.9	−1063.5
	coprecipitation experiments (pH 8) from Zhong (1993); Zhong and Mucci (1995)						
sz-126	−2922.2	−1363.6	−1993.9	−1192.8	−1773.4	−955.5	−1041.0
sz-127	−2923.5	−1364.1	−1994.5	−1192.7	−1774.5	−955.4	−1041.2
sz-116	−2923.1	−1364.0	−1994.3	−1192.7	−1774.3	−955.4	−1041.1
sz-118	−2918.9	−1362.1	−1992.5	−1190.3	−1772.9	−953.1	−1039.0
sz-124	−2921.0	−1363.2	−1993.6	−1191.5	−1774.0	−954.2	−1040.1
sz-123	−2921.0	−1363.3	−1993.7	−1191.5	−1774.1	−954.2	−1040.1
sz-122	−2921.6	−1363.8	−1994.2	−1192.4	−1774.3	−955.1	−1040.9
sz-117	−2920.0	−1363.2	−1993.6	−1191.4	−1773.9	−954.2	−1040.0
sz-114	−2921.9	−1364.1	−1994.5	−1192.3	−1774.9	−955.1	−1041.0
sz-113	−2922.8	−1364.5	−1994.9	−1192.6	−1775.4	−955.4	−1041.3
sz-199	−2921.8	−1364.4	−1995.0	−1192.8	−1774.9	−955.6	−1041.4
hs-208	−2921.2	−1364.1	−1994.8	−1192.6	−1774.6	−955.4	−1041.1
hs-205	−2920.7	−1363.9	−1994.5	−1192.3	−1774.4	−955.1	−1040.9
sz-115	−2924.8	−1366.1	−1996.5	−1194.4	−1776.8	−957.2	−1043.0
hs-206	−2922.9	−1365.4	−1996.1	−1194.0	−1775.8	−956.7	−1042.5
sz-202	−2922.2	−1365.3	−1996.0	−1193.7	−1776.0	−956.4	−1042.3

All values were calculated from elemental normalized chemical potentials (reported in Table 2, 3 and 4). Means and standard deviations are given in Table 8.

Table 8. Means and statistical uncertainties of DualTh standard free energy estimates for the three datasets considered in this study.

Summary statistics for G^*_α of candidate end-members at T = 25°C and p = 1 bar (kJ mol^{-1})	$Eu_2(CO_3)_3$	$Eu(OH)CO_3$	$EuNa(CO_3)_2$	$Eu(OH)_3$	$EuH(CO_3)_2$	$EuO(OH)$	$EuO(CO_3)_{0.5}$
recrystallization experiments (pH 13), this work							
mean	−3106.6	−1425.5	−2088.8	−1193.3	−1896.6	**−956.1**	−1072.2
± σ	6.0	1.7	1.7	1.7	1.7	1.7	1.7
coprecipitation experiments (pH 6), Lakshtanov and Stipp (2004)							
mean	−2939.9	−1379.0	−2010.2	−1221.7	**−1775.1**	−984.6	−1063.2
± σ	4.6	2.0	2.3	2.1	2.0	2.0	2.3
coprecipitation experiments (pH 8), Zhong (1993); Zhong and Mucci (1995)							
mean	−2921.8	−1364.1	−1994.5	−1192.5	**−1774.6**	**−955.3**	−1041.0
± σ	1.4	1.0	1.0	1.0	1.0	1.0	1.0

The sampled G^*_α-values are reported in Table 7.

members (with $CaCO_3$ as Ca pole), failed to reproduce the three datasets simultaneously, regardless of the selected G^*-values.

Three examples of results from the GEM model calculations corresponding to single points on the isotherms shown in Figure 7 are given in Table 10. These results, which are complementary to the speciations listed in Table 6, indicate that for the pH 8 data, the solid solution composition is accounted for by almost equivalent contributions of the two Eu end-members (comparable mole fractions). In contrast, at pH 6 only the $EuH(CO_3)_2$ end-member contributes to the total mole fraction, whereas at pH 13 only the EuO(OH) end-member is relevant.

Thus, our thermodynamic analysis supports the assumption that two distinct Eu species may coexist in calcite. The first, $EuH(CO_3)_2$, arises from the coupled substitution of 2 Ca^{2+} by one Eu^{3+} ion and a proton and is favored at low pH and high pCO_2. It cannot be excluded that the formation of such a complex in calcite is favored by the existence of unidentified aqueous carbonate complexes (e.g., $EuHCO_3^{2+}$). The second Eu species in calcite has the generic stoichiometry $EuO_{x/2}(OH)_{3-x}$ and its incorporation is favored at high pH and low pCO_2.

5. DISCUSSION

5.1. Possible Substitution Mechanisms

Results of our thermodynamic modeling limit the possible substitution mechanisms operating during the uptake of Eu(III) in calcite. Incorporation via the coupled substitution $Na^+ + Eu^{3+} \rightleftharpoons 2\ Ca^{2+}$ as well as incorporation of Eu-Eu pairs on neighboring octahedral sites can be ruled out based on inconsistent model predictions.

The +1 slope of the isotherms clearly favors Eu^{3+} incorporation as an isolated cation, i.e., as mononuclear species surrounded only by Ca^{2+} cations in the adjacent octahedral shell. Additional support to this view is provided by the recent EXAFS study of Elzinga et al. (2002), who investigated Nd(III) and Sm(III) doped calcites and found no evidence of REE(III) backscatterers. In addition, they obtained satisfactory fits to their spectra assuming the usual six Ca neighbors, with REE-Ca distances very close to the Ca-Ca distances of the ideal calcite structure. Thus, their data do not support the hypothesis of vacant octahedral sites adjacent to Eu.

Table 9. End-member solubility products derived from DualTh calculations for the three experimental studies considered in this paper.

Reaction	log K^o_{sp}, derived from . . . coprecipitation experiments (pH ∼ 6)[1]	coprecipitation experiments (pH ∼ 8)[2]	recrystallization experiments (pH ∼ 13)[3]	solubility studies
$Eu_2(CO_3)_3 = 2\ Eu^{3+} + 3\ CO_3^{2-}$	−36.3 ± 0.6	−33.1 ± 0.3	−65.5 ± 1.1	−35.0 ± 0.3
$EuNa(CO_3)_2 = Eu^{3+} + Na^+ + 2\ CO_3^{2-}$	−20.7 ± 0.3	−17.9 ± 0.2	−34.4 ± 0.3	−20.5 ± 0.7
$EuOH(CO_3) = Eu^{3+} + OH^- + CO_3^{2-}$	−20.9 ± 0.4	−18.3 ± 0.2	−29.0 ± 0.3	−21.7 ± 0.1
$Eu(OH)_3 + 3\ H^+ = Eu^{3+} + 3\ H_2O$	11.3 ± 0.4	**16.4 ± 0.2**	**16.2 ± 0.3**	14.9 ± 0.3 (cr) 17.6 ± 0.8 (am)
$EuO(OH) + 3\ H^+ = Eu^{3+} + 2\ H_2O$	11.2 ± 0.4	**16.4 ± 0.2**	**16.2 ± 0.3**	—
$EuO(CO_3)_{0.5} + 2\ H^+ = Eu^{3+} + 0.5\ CO_3^{2-} + H_2O$	2.2 ± 0.4	6.1 ± 0.2	0.6 ± 0.3	—
$EuH(CO_3)_2 = Eu^{3+} + H^+ + 2\ CO_3^{2-}$	**−25.4 ± 0.4**	**−25.3 ± 0.2**	−46.6 ± 0.3	—

The following auxiliary free energies of formation (kJ mol^{-1}), taken from Hummel et al. (2002), were used: $G^o(Eu^{3+})$ = −574.463, $G^o(Na^+)$ = −261.881, $G^o(H_2O, 1)$ = −273.183, $G^o(OH^-)$ = −157.27, $G^o(CO_3^{2-})$ = −527.982. Where available, constants derived from solubility measurements are also given for comparison in the rightmost column (see Table 5 for references). Mutually consistent constants are outlined in bold.

[1](Lakshtanov and Stipp, 2004); [2](Zhong, 1993); [3]this study.

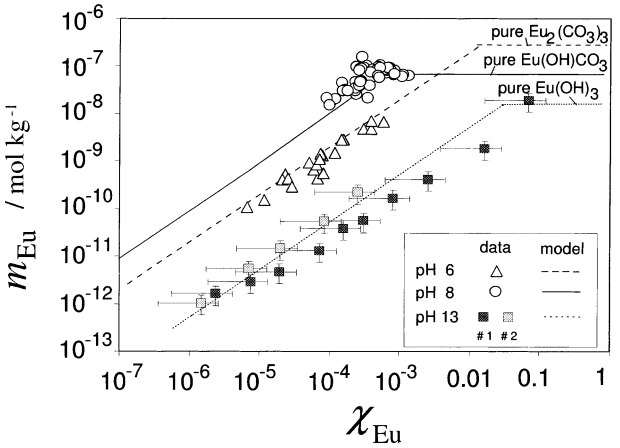

Fig. 7. Ternary EuO(OH) – $EuH(CO_3)_2$ – $CaCO_3$ solid solution model (GEM calculations) compared with Eu-calcite coprecipitation and recrystallization data obtained under widely different pH and pCO_2 conditions. The horizontal lines define the solubility limits set by the least soluble pure Eu solid for the relevant experimental conditions.

Our results indicate that an overall fit of all available data can be obtained only if the formation of a ternary solid solution with $EuH(CO_3)_2$ and a CO_3-free end-member with the generic formula $EuO_{x/2}(OH)_{3-x}$ is assumed. Accordingly, two distinct incorporation mechanisms may be postulated, one involving the coupled substitution $H^+ + Eu^{3+} \rightleftharpoons 2\ Ca^{2+}$ (favored at low pH and high pCO_2) and the other involving the substitution of an Eu oxy-hydroxo complex for Ca^{2+} (favored at high pH and low pCO_2). The latter mechanism requires significant rearrangements of the calcite structure in the vicinity of the substituted Eu ions. Such rearrangements should be feasible, considering the absence of edge-sharing octahedra and bidentate bonds: the calcite lattice consists of a "flexible" three-dimensional network of corner-shared [CaO_6] octahedra that can easily respond to local strain, thus facilitating structural deformations.

Evidence for the deformability of the calcite structure is provided by the recent molecular modeling studies of Fisler et al. (2000) and Cygan et al. (2002). Their molecular models, which accounted for electronic polarization of the oxygens in the carbonate groups, reveal that a vacancy in octahedral position (a negative charge defect) would induce important structural distortion around the site. Specifically, intermolecular distances between oxygens belonging to different CO_3^{2-} groups are predicted to distribute in a continuum between 2.9 and 3.5 Å, whereas in the undisturbed calcite structure three discrete distances are found at 3.2, 3.3 and 3.4 Å. Even intramolecular distances, i.e., the distances between oxygens belonging to the same carbonate group, are predicted to change.

According to the calculated solution speciation (Fig. 6, Table 6), the dominant Eu aqueous species at pH 6 ($pCO_2 \sim 1$ bar) is predicted to be $Eu(CO_3)^+$, whereas the hydroxo species $Eu(OH)_4^-$ prevails at pH 13 ($pCO_2 \sim 0$). Thus, there seems to be a correlation between the speciation of Eu in the parent solution and the two inferred Eu environments in calcite (one with neighboring CO_3^{2-} groups, the other only coordinated by free O^{2-}/OH^-). This, in turn, suggests that the two different coordination environments of Eu in the calcite lattice could be inherited from adsorption of the dominant Eu aqueous species at the specific chemical conditions of the experiment.

5.2. Thermodynamic Model vs. Spectroscopic Data

The picture emerging from our thermodynamic study is also consistent with the laser fluorescence data of Stumpf and Fanghänel (2002), who found two distinct coordination environments for Cm(III)—a chemical analog of Eu(III)—in a natural calcite recrystallized in the presence of trace amounts of this trivalent actinide. Of the two Cm(III) species identified in calcite, one is partially hydrated (one H_2O or OH^- in the first coordination sphere), whereas the other is completely dehydrated. Stumpf and Fanghänel (2002) first interpreted the hydrated Cm(III) species as a surface complex, whereas the dehydrated species was explained as Cm(III) substituted in octahedral position. New unpublished laser fluorescence data confirm the existence of two analogous Eu(III) species both in synthetic and natural calcites and suggest that the hydrated species is not a surface complex, but rather a complex substituted in the bulk structure (T. Stumpf, private communication).

Supplemental evidence for the existence of two distinct REE species in calcite comes from the EXAFS study of Elzinga et al. (2002), whose results have been recently confirmed by Whiters et al. (2003). Both Nd^{3+} and Sm^{3+} were found to occupy the octahedral position, but the first-shell REE-O distances were determined to be larger (+ 0.05 Å) than the corresponding Ca-O distances in pure calcite, despite the smaller ionic radii of Nd^{3+} and Sm^{3+}. Moreover, an increased first-shell coordination number (~ 7 instead of 6) was inferred from the analysis of the EXAFS spectra. The authors suggested that the increased coordination number may result from the formation of a bidentate bond between the REE^{3+} ion and a CO_3^{2-} group. Alternatively, the EXAFS results of Elzinga et al. (2002) can also be interpreted by a mixture of two species, one with CN = 6, the other with higher CN = 9. This interpretation would also be consistent with our two-species model for Eu in calcite.

This scenario is corroborated by independent crystallo-

Table 10. Selected results obtained with the ternary $EuH(CO_3)_2$ – EuO(OH) – $CaCO_3$ solid solution model (GEM calculations).

Parameter	pH 6	pH 8	pH 13
total Eu in system, m^0_{Eu} (mol kg^{-1})	10^{-6}	10^{-6}	10^{-6}
dissolved Eu at equilibrium, m_{Eu} (mol kg^{-1})	1.6×10^{-9}	6.3×10^{-8}	1.6×10^{-8}
$\chi_{EuH(CO_3)_2}$	1.6×10^{-4}	4.5×10^{-4}	0
$\chi_{EuO(OH)}$	1.3×10^{-9}	3.5×10^{-4}	3.2×10^{-2}

Total added Eu (m^0_{Eu}), equilibrium molalities (m_{Eu}) and Eu end-member mole fractions are given. These results are complementary to the speciation calculations presented in Table 6.

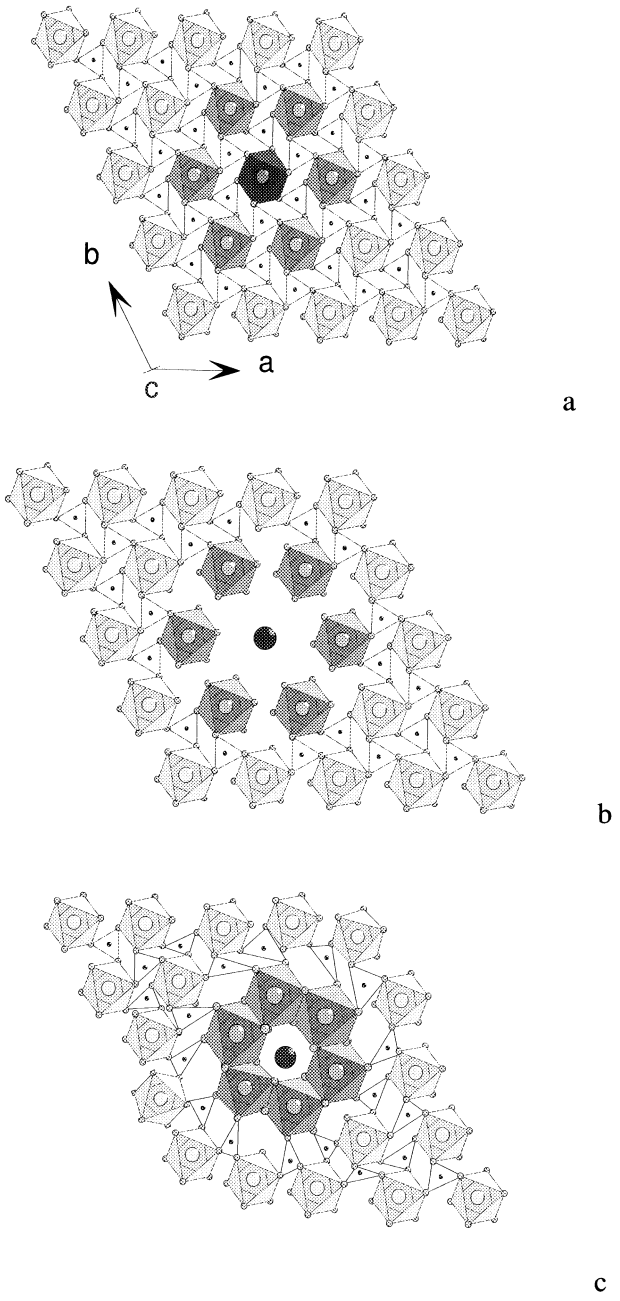

Fig. 8. Possible formation mechanism for a $EuO_{x/2}(OH)_{3-x}$ complex in calcite. Detailed explanations are given in section 5.3.

graphic data, that yield a coordination number of 9 for $REE(OH)_3$ and interatomic distances in the 2.50–2.52 Å range (Beall et al., 1977), i.e., an increment of + 0.14–0.16 Å with respect to Ca-O distances in pure calcite. Consistent with our ternary model, the + 0.05 Å excess determined by the EXAFS fitting procedure could be interpreted as a result of a mixture of two distinct Nd complexes, one with a short Nd-O distance similar to Ca-O in calcite, the other with a longer Nd-O distance similar to that found in hexagonal $Nd(OH)_3$.

5.3. Atomic Scale Model for Europium Oxy-Hydroxide End-Member

It is not yet possible, based on the available thermodynamic and spectroscopic evidence, to resolve the geometry of the coordinative rearrangements that take place following the incorporation of Eu in calcite. Nevertheless, a relatively simple mechanism of structural accommodation can be envisaged to explain, at least qualitatively, the formation of the proposed $EuO_{x/2}(OH)_{3-x}$ end-member species, which requires "free" (non-carbonate) oxygens in the first coordination shell of Eu^{3+}.

The possible mechanism is illustrated in Figure 8 as a sequence of three "snapshots" that illustrate the proposed local change in the calcite structure upon Eu^{3+} incorporation. In Figure 8a, a fragment of the undisturbed calcite structure projected on the plane perpendicular to the c-axis is shown. The central octahedron in black denotes the hypothetical site where substitution with Eu^{3+} takes place. The six surrounding $[CaO_6]$ octahedra are also highlighted in medium grey. If each of the octahedra surrounding the central site "loses" four of the six carbonate groups (Fig. 8b), and the structure collapses into a hexagonal ring of edge-sharing octahedra, then a cavity with the required nine-fold coordination of Eu^{3+} is formed (Fig. 8c). Each of the nine oxygens coordinating the central Eu^{3+} cation is shared among three octahedra (the third one, not shown, in the c-axis direction), so that a stoichiometric O:Eu ratio of 9:3, consistent with the $Eu(OH)_3$ stoichiometry, would result.

6. CONCLUSIONS

The main conclusion from this study is that heterovalent substitution of Eu in calcite cannot be described with binary isomorphic solid solution models. The processes involved are more complex than in the case of homovalent substitutions. The different chemical properties of substituent and substituted ion and the need to neutralize the charge imbalance introduced through heterovalent substitutions may induce, on a molecular scale, considerable coordinative rearrangements in the calcite structure. Only a careful analysis of experimental data collected over a wide range of chemical conditions, combined with adequate spectroscopic data, allows us to unravel the substitution processes involved in the formation of heterovalent solid solutions. On the basis of the thermodynamic analysis carried out in this study and spectroscopic evidence, at least two distinct substitution mechanisms must be considered to explain the formation of dilute Eu-calcite solid solutions, depending on chemical conditions. Our data suggest that the coupled substitution $H^+ + Eu^{3+} = 2\ Ca^{2+}$ prevails at low pH and high pCO_2, possibly following adsorption of Eu-bicarbonate complexes. In alkaline systems at very low pCO_2, an Eu oxy-hydroxo group is preferentially incorporated into calcite, reflecting the dominance of the Eu hydroxo species in solution.

Our ternary solid solution model also proved to agree qualitatively with the results of spectroscopic and molecular modeling studies. Notwithstanding these encouraging results, further investigations—especially of spectroscopic nature—are necessary to substantiate our findings.

Acknowledgments—This study was partly carried out for the ACTAF project, within the 5th European framework program for Research and

Development of the European Commission. The Swiss Federal Office for Education and Science (BBW) and the National Cooperative for the Disposal of Radioactive Waste (Nagra) are gratefully acknowledged for their financial contributions. Special thanks are due to L. Lakshtanov and S. Stipp, who kindly shared with us their experimental results. We are also grateful to S. Zhong and A. Mucci for providing us details of their experiments and to T. Stumpf and M. Marques-Fernandes for fruitful discussions and details related to their current work. Finally, we are indebted to the three anonymous reviewers and to the associate editor for their constructive criticism, which greatly helped in revising this manuscript.

Associate editor: A. Mucci

REFERENCES

Beall G. W., Milligan W. O., and Wolcott H. A. (1977) Structural trends in the lanthanide trihydroxides. *J. Inorg. Nucl. Chem.* **39,** 65–70.

Bernkopf M. F. (1984) Hydrolysereaktionen und Karbonatkomplexierung von dreiwertigem Americium im natürlichen aquatischen System. Ph.D. thesis, Technische Universität München.

Bevington P. R. (1969) Data reduction and error analysis for the physical sciences. McGraw-Hill, New York.

Carlsson T., and Aalto H. (1997) Coprecipitation of Ni with calcite: an experimental study. In *Scientific Basis for Nuclear Waste Management XXI* (eds. I. G. McKinley, and Ch. McCombie). Mat. Res. Soc. Symp. Vol. 506, pp. 621–627. Materials Research Society, Warrendale, Pensylvania.

Carroll S. A. (1993) Precipitation of Nd-Ca carbonate solid solution. *Geochim. Cosmochim. Acta* **57,** 3383–3393.

Curti E. (1999) Coprecipitation of radionuclides with calcite: estimation of partition coefficients based on a review of laboratory investigations and geochemical data. *Appl. Geochem.* **14,** 433–445.

Cygan R. T., Wright K., Fisler D. K., Gale J. D., and Slater B. (2002) Atomistic models of carbonate minerals: Bulk and surface structures, defects and diffusion. *Mol. Simul.* **28,** 475–495.

Davis J. A., Fuller C. C., and Cook A. D. (1987) A model for trace metal sorption processes at the calcite surface: adsorption of Cd^{2+} and subsequent solid solution formation. *Geochim. Cosmochim. Acta* **51,** 1477–1490.

Elzinga E. J., Reeder R. J., Withers S. H., Peale R. E., Mason R. A., Beck K. M., and Hess W. P. (2002) EXAFS study of rare-earth element coordination in calcite. *Geochim. Cosmochim. Acta* **66,** 2875–2885.

Fannin C. A (1999) The rare earth elements as natural analogues for the actinides. Ph.D. thesis, John Moores University, Liverpool.

Fannin C. A., Edwards R., Pearce J., and Kelly E. (2002) A study on the effects of drying conditions on the stability of $NaNd(CO_3) \cdot 2.6\ H_2O$ and $NaEu(CO_3)_2 \cdot 2.6\ H_2O$. *Appl. Geochem.* **17,** 1305–1312.

Fisler D. K., Gale J. D., and Cygan R. T. (2000) A shell model for the simulation of rhombohedral carbonate minerals and their point defects. *Am. Mineral.* **85,** 217–224.

Gamsjäger H. (1985) Solid state chemical model on the solubility behaviour of homogeneous solid Co-Mn-carbonate mixtures. *Ber. Bunsenges. Phys. Chem.* **89,** 1318–1322.

Gamsjäger H., Königsberger E., and Preis W. (2000) Lippmann Diagrams: Theory and application to carbonate systems. *Aqua. Geochem.* **6,** 119–132.

Glynn P. D. (1991) MBSSAS: A computer code for the computation of Margules parameters and equilibrium relations in binary solid-solution aqueous-solution systems. *Comp. Geosci.* **17,** 907–966.

Glynn P. D. (2000) Solid-solution solubilities and thermodynamics: sulfates, carbonates and halides. In *Sulfate minerals: crystallography, geochemistry and environmental significance* (eds. C. N. Alpers, J. L. Jambor, and D. K. Nordstrom), pp. 481–510. Rev. in Mineralogy, Vol. 40, Mineralogical Society of America and Geochemical Society, Washington D.C.

Glynn P. D., Reardon E. J., Plummer L. N., and Busenberg E. (1990) Reaction paths and equilibrium end-points in solid-solution aqueous-solution systems. *Geochim. Cosmochim. Acta* **54,** 267–282.

Hummel W., Berner U., Curti E., Pearson F. J., and Thoenen T. (2002) *Nagra/PSI Chem. Thermodynamic Data Base 01/01*. Nagra Technical Report NTB 02-16, Nagra, Wettingen, Switzerland and Universal Publishers/uPublish.com, Parkland, Florida, ISBN 1–58112–620–624.

Karpov I. K., Chudnenko K. V., and Kulik D. A. (1997) Modeling chemical mass-transfer in geochemical processes: Thermodynamic relations, conditions of equilibria and numerical algorithms. *Am. J. Sci.* **297,** 767–806.

Karpov I. K., Chudnenko K. V., Kulik D. A., Avchenko O. V., and Bychinskii V. A. (2001) Minimization of Gibbs free energy in geochemical systems by convex programming. *Geochem. Int.* **39,** 1108–1119.

Kulik D. A., and Kersten M. (2002) Aqueous solubility diagrams for cementitious waste stabilization systems: 4. A carbonation model for Zn-doped calcium silicate hydrate by Gibbs energy minimization. *Environ. Sci. Technol.* **36,** 2926–2931.

Kulik D. A., Kersten M., Heiser U., and Neumann T. (2000) Application of Gibbs energy minimization to model early-diagenetic solid-solution aqueous-solution equilibria involving authigenic rhodochrosites in anoxic Baltic Sea sediments. *Aqua. Geochem.* **6,** 147–199.

Kulik D. A. (2002) Gibbs energy minimization approach to modeling sorption equilibria at the mineral-water interface: Thermodynamic relations for multi-site-surface complexation. *Am. J. Sci.* **302,** 227–279.

Lakshtanov L., and Stipp S. (2004) Experimental study of europium (III) coprecipitation with calcite. *Geochim. Cosmochim. Acta* **68,** 819–827.

McIntire W. L. (1963) Trace element partition coefficients—a review of theory and applications to geology. *Geochim. Cosmochim. Acta* **27,** 1209–1264.

Mucci A., and Morse J. W. (1984) The solubility of calcite in seawater solutions of various magnesium concentrations, $I_t = 0.697$ m at 25 degrees C and one atmosphere total pressure. *Geochim. Cosmochim. Acta* **48,** 815–822.

NAGRA (2002) *Project Opalinus Clay—Safety Report: Demonstration of disposal feasibility for spent fuel, vitrified high-level waste and long-lived intermediate-level waste (Entsorgungsnachweis)*. Nagra Technical Report NTB 02–05, National Cooperative for the Disposal of Radioactive Waste (NAGRA), Wettingen, Switzerland.

Parkhurst D. L., and Appelo C. A. J. (1999) *User's guide to PHREEQC (version 2)—A computer program for speciation, batch-reaction, one-dimensional transport and inverse geochemical calculations*. Water-resources investigation report 99–4259, United States Geological Survey, Denver, Colorado.

Runde W., Meinrath G., and Kim J. I. (1992) A study of solid-liquid phase equilibria of trivalent lanthanide and actinide ions in carbonate systems. *Radiochim. Acta* 58/59, 93–100.

SKB (1999) *SR 97—Waste, repository design and sites. Background report to SR 97*. Swedish Nuclear Fuel and Waste Management Co. (SKB). SKB Report TR-99–08, Stockholm, Sweden.

Strunz H., and Nickel E. H. (2001) *Strunz mineralogical tables (chemical structural mineral classification system)*. E. Schweizerbart'sche Verlagsbuchhandlung (Nägele u. Obermiller), Stuttgart, Germany.

Stumpf T., and Fanghänel T. (2002) A time-resolved laser fluorescence spectroscopy (TRLFS) study of the interaction of trivalent actinides (Cm(III)) with calcite. *J. Coll. Interf. Sci.* **249,** 119–122.

Terakado Y., and Masuda A. (1988) The coprecipitation of rare-earth elements with calcite and aragonite. *Chem. Geol.* **69,** 103–110.

Tesoriero A. J., and Pankow J. F. (1996) Solid solution partitioning of Sr^{2+}, Ba^{2+} and Cd^{2+} to calcite. *Geochim. Cosmochim. Acta* **60,** 1053–1063.

Thorstenson D. C., and Plummer L. N. (1977) Equilibrium criteria for two-component solids reacting with fixed composition in an aqueous phase; example: the magnesian calcites. *Am. J. Sci.* **277,** 1203–1223.

Tits J., Wieland E., Bradbury M. H., Eckert P., and Schaible A. (2002) The uptake of Eu(III) and Th(IV) by calcite under hyperalkaline conditions. PSI-Bericht Nr. 02-03 (ISSN 1019-0643), Paul Scherrer Institut, Villigen, Switzerland.

Whiters S. H., Peale R. E., Schulte A. F., Braunstein G., Beck K. M., Hess W. P., and Reeder R. J. (2003) Broad distribution of crystal-

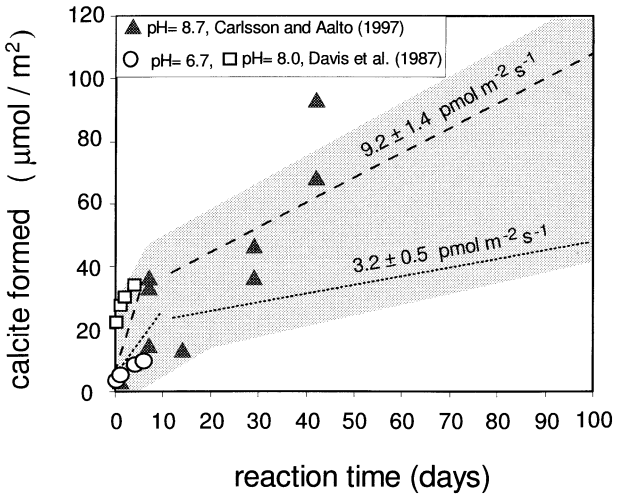

Fig. A1.1. Comparison of recrystallization rates derived in this study (average trend lines and shaded area, see Fig. 1) with other published data on ^{45}Ca uptake (symbols) during calcite recrystallization.

field environments for Nd^{3+} in calcite. *Phys. Chem. Min.* **30,** 440–448.

Zhong S. (1993) Precipitation kinetics and partitioning of rare earth elements (REE) between calcite and seawater. Ph.D. thesis, McGill University, Montreal.

Zhong S., and Mucci A. (1995) Partitioning of rare earth elements (REEs) between calcite and seawater solutions at 25°C and 1 atm and high dissolved REE concentrations. *Geochim. Cosmochim. Acta* **59,** 443–453.

APPENDIX 1

To determine the amount of recrystallized calcite from ^{45}Ca activity measurements, one must take into account that: (i) radioactive decay cannot be neglected, since the half-life of ^{45}Ca (163.1 days) is comparable to the duration of the experiments (up to 90 days); (ii) the ratio of ^{45}Ca to total Ca in solution also changes due to calcite dissolution during recrystallization. This leads to the following two-term mass balance equation:

$$\frac{\partial m_{45}}{\partial t} = -\lambda m_{45} - \frac{1}{W}\frac{\partial n}{\partial t}\frac{m_{45}}{m_{Ca}} \qquad \text{(A1.1)}$$

where m_{45} is the ^{45}Ca tracer molality, λ is the decay constant, m_{Ca} is the total calcium molality (constant because of calcite saturation), W is the mass of water solvent, n the amount in moles of newly formed calcite, and t is the reaction time. Eqn. (A1.1) simply states that the ^{45}Ca concentration decreases due to the combined effect of radioactive decay and incorporation in the newly formed calcite. It is a first-order partial differential equation with two time-dependent variables, m_{45} and n, with the following solution for the initial condition $n = 0$:

$$n = W\, m_{Ca}\left(\ln\frac{m^o_{45}}{m_{45}} - \lambda\, t\right) \qquad \text{(A1.2)}$$

where m_{45} is the initial ^{45}Ca concentration. Eqn. (A1.2) gives the amount of recrystallized calcite as a function of the ^{45}Ca tracer concentration measured in solution at any reaction time t.

The recrystallization rates listed in Table 1 were derived from our data by applying Eqn. (A1.2). They are comparable to those found with the same ^{45}Ca uptake method by Davis et al. (1987) and Carlsson and Aalto (1997) (Fig. A1.1), although these investigations were carried out at lower pH. Thus, the available ^{45}Ca data indicate that all measured calcite recrystallization rates fall within a restricted range despite widely different pH and S/W conditions.

The latter observation is important since our Eu uptake experiments were conducted at a lower S/W (0.5 g l^{-1}) than the ^{45}Ca exchange experiments. Unfortunately, it was not possible to determine the recrystallization rate at 0.5 g l^{-1} because of the very weak ^{45}Ca uptake at such low S/W ratios. Thus, we had to extrapolate the amount of calcite recrystallized during the Eu uptake experiments (14 days reaction time) from data obtained at higher S/W ratios and reaction times between 7 and 42 days. We estimated that 25.5 ± 9.9 μmol of calcite per kg of solution recrystallized, which leads to not more than one order of magnitude uncertainty in the Eu mole fractions.

The reasons for the observed dependency of recrystallization rates on S/W ratios are not well understood. We suspect that this phenomenon might be related to the presence of (unidentified) inhibitors: one may argue that when the S/W ratio is reduced, the inhibitor concentration per unit mineral surface area increases, which would lead to a larger fraction of active growth sites blocked by the inhibitor on the mineral surface.

APPENDIX 2

In section 4.2 we suggested that the slope of the linear isotherms plotted in Figure 2 is related to the substitution process taking place during the formation of dilute Eu-calcite solid solutions. Here, we demonstrate how the isotherm's slope depends on the stoichiometry of the substituted entity at trace concentrations.

If, for instance, Sr^{2+} substitutes for Ca^{2+} as *single* isolated cations dispersed in the calcite lattice (each Sr^{2+} cation being surrounded by 6 Ca^{2+}), then a monomeric Sr end-member stoichiometry must be defined, i.e., the solid solution is formally defined through the end-members $SrCO_3$ and $CaCO_3$. In contrast, if the Sr^{2+} cations are incorporated as *pairs* in adjacent octahedral sites, one must accordingly define end-members with dimeric stoichiometry, i.e., $Sr_2(CO_3)_3$-$Ca_2(CO_3)_2$. It is important to realize that these alternative definitions are not merely scaling factors, but characterize solid solutions with different thermodynamic properties. The mixing entropy of the $SrCO_3$-$CaCO_3$ solid solution will be considerably larger than for dimeric end-members, because the number of possible permutations per mole of $(Ca,Sr)CO_3$ will be higher.

In the case of heterovalent substitution, there is a further complication due to the requirement of local charge balance. As one of many possible solid solution configurations, it can be assumed that the excess electrical charge introduced by trivalent or higher charged cations is locally balanced by contiguous vacancies. For instance, three adjacent Ca^{2+} ions could be replaced by two Eu^{3+} ions and a vacancy ($3\ Ca^{2+} = 2Eu^{3+} + \square$), implying $Eu_2(CO_3)_3$-$Ca_3(CO_3)_3$ bulk end-member stoichiometries. Alternatively, local charge balance may be achieved through the substitution $Ca^{2+} = Eu^{3+} + OH^-$, which requires $Eu(OH)CO_3$ and $CaCO_3$ as end-members, or through coupled substitution with a monovalent cation (Na^+-Eu^{3+} or H^+-Eu^{3+} for two Ca^{2+}). A third, more complex mechanism would involve the simultaneous substitution of Eu^{3+} for Ca^{2+} and 3 OH^- for a single CO_3^{2-} group.

The relation between isotherm slope and end-member stoichiometry can be derived directly from law-of-mass-action expressions and approximations that apply to dilute solid solutions. Consider an ideal binary solid solution with end-members B_bYu-C_cY_w, where B and C are the cations, Y is a common anion, b, c, u, w are stoichiometric coefficients and, in the case of heterovalent substitution, $b \neq c$ and/or $u \neq w$. For a dilute solid solution of B_bYu in C_cY_w the following law-of-mass-action expressions describe thermodynamic equilibrium with the aqueous solution:

$$B_bY_u \rightleftharpoons bB^{+Z_B} + uY^{-Z_Y} \quad K^o_{B_bY_u} = \frac{a_B^b\, a_Y^u}{\gamma_{B_bY_u}\ \chi_{B_bY_u}} \qquad \text{(A2.1)}$$

$$C_cY_w \rightleftharpoons cC^{+Z_C} + wY^{-Z_Y} \quad K^o_{C_cY_w} = \frac{a_C^c\, a_Y^w}{\gamma_{C_cY_w}\ \chi_{C_cY_w}} \qquad \text{(A2.2)}$$

$K^o_{B_bY_u}$ and $K^o_{C_cY_w}$ are the end-member solubility products at zero ionic strength, a_B a_C, a_Y are the ionic activities of B^{+Z_B},C^{+Z_C} and Y^{-Z_Y}, respectively, $\chi_{B_bY_u}$, $\chi_{C_cY_w}$ are end-member mole fractions and $\gamma_{B_bY_u}$, $\gamma_{C_cY_w}$ are the corresponding activity coefficients. In the case of a dilute solid solution the approximations $\chi_{C_cY_w} \cong \gamma_{C_cY_w} \cong 1$ (major end-member) and $\gamma_{C_cY_w} \cong cons$ (minor end-member) hold. The mole

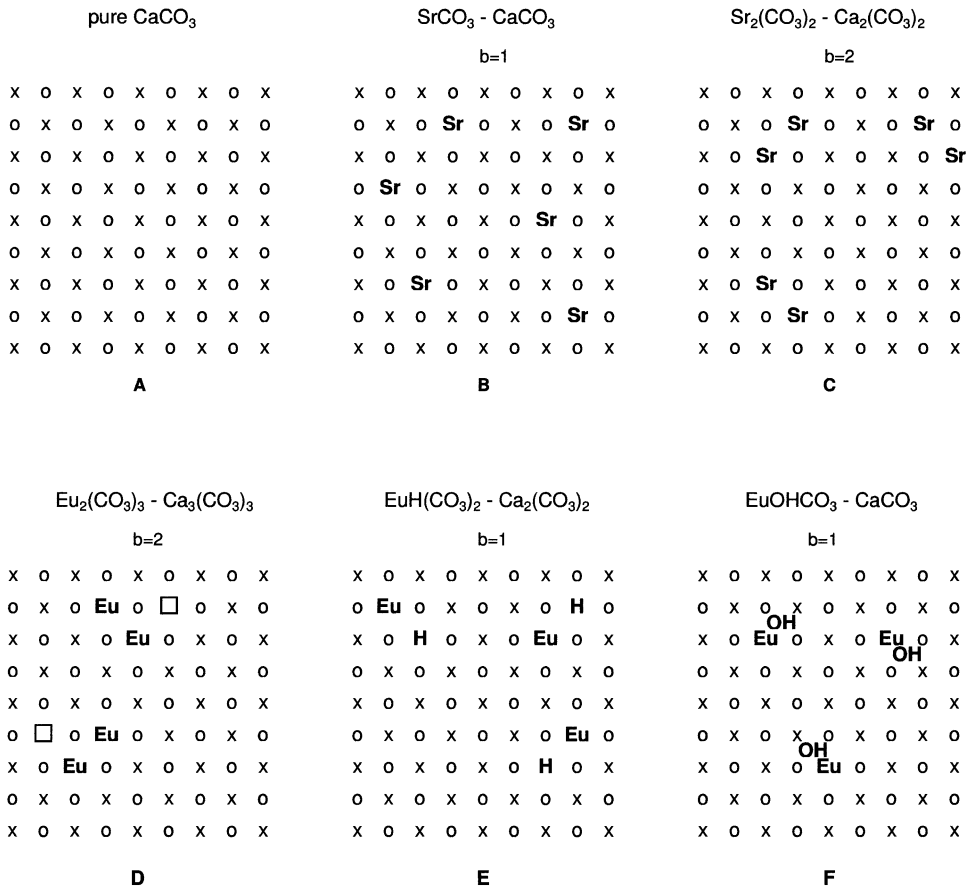

Fig. A2.1. Schematic representation of calcite lattice (x = Ca^{2+}, o = CO_3^{2-}) and possible cation substitution mechanisms: (A) undisturbed lattice, (B) homovalent substitution of isolated Sr^{2+} cations, (C) homovalent substitution of dimeric $(Sr^{2+})_2$ groups, (D) substitution of dimeric $(Eu^{3+})_2$ groups adjacent to vacant octahedral sites, (E) coupled H^+-Eu^{3+} substitution, (F) substitution of $EuOH^{2+}$ groups. The corresponding solid solution end-members and the value of the stoichiometric parameter b in Eq. (A2.6) are shown above each sketch.

fraction of the dilute component is Ther given by:

$$\chi_{B_bY_u} \cong \frac{n_{B_bY_u}}{n_{C_cY_w}} = \frac{n_B/b}{n_C/c} = \frac{c}{b}\,\chi_B \tag{A2.3}$$

where n_B, n_C are moles of the cations B^{+Z_B} and C^{+Z_C}, respectively, in the solid solution and χ_B is the cationic mole fraction of B^{+Z_B} (Eqn. 8). Eqn. (A2.3) shows that the conversion between end-member and cationic mole fractions depends on the stoichiometry of *both* end-members (coefficients b, c). The solubility product of the dilute end-member, see Eqn. (A2.1), will thus also depend on the stoichiometric coefficients of both end-members when expressed as a function of the cationic mole fraction:

$$K^o_{B_bY_u} = \frac{a_B^b\, a_Y^u}{\gamma_{B_bY_u}\,\chi_B}\;\frac{b}{c} \tag{A2.4}$$

For a series of experiments carried out under constant conditions only the amount of trace cation B added to the solution (Eu in our case) is varied in each experiment to establish an isotherm. Hence only a_B and χ_B vary in the previous equation, while all other quantities are constant. Introducing activity coefficients, γ_i, and the speciation factor, ϕ_B, defined as the fraction of total dissolved element B present as free (non-complexed) ion, Eqn. (A2.4) can be expanded as follows:

$$\log K^o_{B_bY_u} = b\,\log(\gamma_B\phi_B m_B) + u\,\log a_Y + \log\frac{b}{c} - \log\gamma_{B_bY_u} - \log\chi_B \tag{A2.5}$$

Collecting all constant terms under k (γ_B and ϕ_B can also be taken as constant for a dissolved trace element) one obtains:

$$\log m_B = k + \frac{1}{b}\log\chi_B \tag{A2.6}$$

where

$$k = \frac{\log K^o_{B_bY_u}}{b} - \log(\gamma_B\phi_B) - \frac{u}{b}\log a_Y - \frac{1}{b}\log\frac{b}{c} + \frac{1}{b}\log\gamma_{B_bY_u} \tag{A2.7}$$

Eqn. (A2.6) is a linear equation with a slope $1/b$ and intercept k, where the slope defined by a series of data on an isotherm plot (e.g., Fig. 2) is inversely proportional to the stoichiometric coefficient of the trace end-member formula. Accordingly, for the substitution 3 Ca^{2+} = 2 Eu^{3+} + □, a slope of + 1/2 would result in the plot of Figure 2. Since the slopes defined by the experimental isotherm data are + 1, one is forced to rule out this substitution mechanism. Eqn. (A2.6) can also be derived from basic principles of statistical mechanics, through a calculation of the configurational entropy of binary ideal mixtures as a function of the stoichiometric coefficient b (derivation not shown).